



M6.4 Paratebueno Earthquake

June 8, 2025

Released: 7/18/2025

NHERI DesignSafe Project ID: PRJ-6007



JOINT RECONNAISSANCE REPORT (JRR)

Joint Reconnaissance Team Leaders:
Jorge Archbold, Universidad del Norte / CEER

Field Assessment Structural Team (FAST):
Lead: Jorge Archbold, Universidad del Norte / CEER
Julian Carrillo, Universidad Militar Nueva Granada / CEER

Virtual Assessment Structural Team (VAST) Section Authors:
(in order of section authored)

Gustavo A. Araújo R., Stanford University
Juan Diego Angulo, Universidad del Norte
Juan Miguel Valois, Stanford University
Carlos Arteta, Universidad del Norte / CEER
Jesus Caballero, Universidad del Norte
Orlando Arroyo, Universidad Industrial de Santander / CEER

Albert Ortiz, Universidad del Valle / CEER
Bayron Salazar, Universidad del Valle
Carlos A. Blandon, Universidad EIA / CEER
Maria Camila Lopez, UC Berkeley
Ricardo Bonnet, Universidad de Medellin / CEER

Report Editors:
(in alphabetical order)
Tracy Kijewski-Correa, University of Notre Dame
Eduardo Miranda, Stanford University
Khalid M. Mosalam, University of California, Berkeley

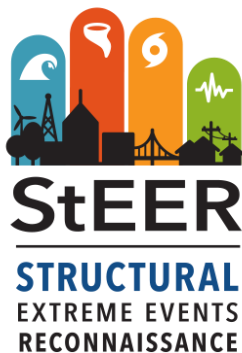


PREFACE



The **Colombian Earthquake Engineering Research Network (CEER)** (see <http://www.ceer.co/>) is a national collaborative initiative dedicated to advancing earthquake engineering research, fostering the development

of high-level technical expertise, and promoting risk reduction and resilience across Colombia. Founded in 2017 by faculty from Universidad del Norte, Universidad EIA, Universidad de Medellín, and Universidad Militar Nueva Granada, CEER brings together academic institutions and researchers to address the impacts of seismic and other natural hazards through coordinated research efforts. CEER strengthens interdisciplinary collaboration, facilitates knowledge exchange, and supports the generation of science-based solutions to mitigate risk and protect communities.



The National Science Foundation (NSF) awarded an EAGER grant (CMMI 1841667) to a consortium of universities to form the **Structural Extreme Events Reconnaissance (StEER) Network** (see <https://www.steer.network> for more details). StEER was renewed through a second award (CMMI 2103550) to further enhance its operational model and develop new capabilities for more efficient and impactful post-event reconnaissance. StEER builds societal resilience by generating new knowledge on the performance of the built environment through impactful post-disaster reconnaissance disseminated to affected communities. StEER achieves this vision by: (1) deepening structural engineers' capacity for post-event reconnaissance by promoting community-driven standards, best practices, and training, as well as their understanding of the effect of natural hazards on society; (2) coordination

leveraging its distributed network of members and partners for early, efficient and impactful responses to disasters; and (3) collaboration that broadly engages communities of research, practice and policy to accelerate learning from disasters.



The **Earthquake Engineering Research Institute (EERI)** is the leading non-profit membership organization dedicated to understanding earthquake risk and increasing earthquake resilience in communities worldwide. Its multidisciplinary membership includes researchers, practitioners, and students in engineering, geoscience, social science, architecture, planning, government, emergency management, public health, and policy making. EERI has been bringing people and disciplines together since 1948. EERI provides members with the technical knowledge, leadership and advocacy skills, collaborative networks, and

multidisciplinary context to achieve earthquake resilience in their communities worldwide. For more information about EERI, please visit: <https://www.eeri.org/>.

COPYRIGHT DISCLAIMER

This report was developed to contribute to the efforts of the international research community with the ultimate goal of understanding certain scientific aspects of the Mw 6.4 Paratebueno Earthquake. No resources included in this report are used for commercial purposes and none of the authors receive remuneration directly related to the publication of this research document.

All external resources in this report were utilized in line with the Berne Convention for the Protection of Literary and Artistic Works, Section 107 of the Copyright Act of 1976, and the practice of the courts in the United States.

All external resources in this report were used in good faith and in consideration of the possibility of 'fair use' which allows otherwise infringing resource usage to be exempted based on the criteria established by the aforementioned regulations and the practice of the courts.

Fair use is a doctrine in United States copyright law that allows limited use of copyrighted material without requiring licensing and permission from the rights holders, such as commentary, criticism, news reporting, research, teaching or scholarship. It provides for the legal, non-licensed citation or incorporation of copyrighted material in another author's work under a four-factor balancing test.

ATTRIBUTION GUIDANCE

Reference to JRR Analyses, Discussions or Recommendations

Reference to the analyses, discussions or recommendations within this report should be cited using the full citation information and DOI from DesignSafe (these are available at <https://www.steer.network/responses>).

Citing Images from this JRR

Some images in this report are taken from public sources. Each figure caption specifies the “Source” attributed to the owner of that image; re-use of the image should cite that source directly. Note that public sources might still have copyright issues and depending on the use case, the user may need to secure additional permissions/rights from the original copyright owner.

Other images in this report were acquired by one of the contributing organizations or their collaborators. Such images are denoted with “Credit” attributed to the individual in the caption. Thus, it is appropriate to use the report’s full citation information and DOI from DesignSafe (these are available at <https://www.steer.network/responses>).



ACKNOWLEDGMENTS

This material is based upon work supported by the National Science Foundation under Grant No. CMMI 2103550. Any opinions, findings, and conclusions or recommendations expressed in this material are those of StEER and do not necessarily reflect the views of the National Science Foundation. All authors and editors listed on the cover page participate as volunteer professionals. Thus, any opinions, findings, and conclusions or recommendations expressed herein are those of the individual contributors and do not necessarily reflect the views of their employer or other institutions and organizations with which they affiliate.

Special thanks are given to Professor Julián Carillo of Universidad Militar Nueva Granada for his invaluable support in coordinating the logistics of our post-earthquake reconnaissance visit to the Paratebueno region. His efforts in securing university funding for transportation, including a vehicle and driver, were instrumental to the success of the fieldwork. We also thank him for obtaining support letters from both the Servicio Geológico Colombiano (SGC) and the Asociación de Ingeniería Sísmica de Colombia (AIS), which enabled us to access government-restricted areas affected by the earthquake.

The sharing of videos, damage reports and briefings via Slack by the entire NHERI community was tremendously helpful and much appreciated. StEER recognizes the efforts of the DesignSafe CI team who continuously supported and responded to StEER's emerging needs.

ACCESS THIS AND OTHER PRODUCTS



For a full listing of reports issued by CEER, please visit the CEER website: <http://ceer.co/reportes-ceer/>



For a full listing of this report and all other StEER products (briefings, reports and datasets) with full citation information and DOIs, please visit the StEER website: <https://www.steer.network/responses>



The Learning from Earthquakes website provides access to this and other Virtual Earthquake Reconnaissance Team (VERT) reports, datasets, and publications from over 300 earthquakes in more than 50 countries:

<http://www.learningfromearthquakes.org/>



COMMON TERMS & ACRONYMS

| Acronym | General Terms | Brief Description |
|---------|---|---|
| -- | DesignSafe | Data Repository |
| -- | DesignSafe-CI | Academic Organization within NHERI |
| AI | Arias Intensity | Intensity Measure |
| ASCE | American Society of Civil Engineers | Professional Organization |
| ASTM | American Society for Testing and Materials (now ASTM International) | Standards Body |
| ATC | Applied Technology Council | Professional Organization |
| BOCA | Building Officials and Code Administrators | Code Body |
| CC-BY | Creative Commons Attribution License | Code/Standard |
| CEER | Colombian Earthquake Engineering Research Network | Academic Organization |
| CESMD | Center for Engineering Strong Motion Data | Governmental Agency |
| CI | Cyberinfrastructure | Research Asset |
| CLPE | Critical Load Path Elements | StEER Term |
| CMU | Concrete Masonry Unit | Building Material |
| CPIC | Center for Public Interest Communication | Research Support Organization within University of Florida to study, test and apply strategic communication for social change |
| CWA | Central Weather Administration | Taiwan Governmental Agency |
| DBE | Design Basis Earthquake | Design Terminology |
| DEQC | Data Enrichment and Quality Control | StEER Term |
| DOI | Digital Object Identifier | Common Term |
| EARR | Early Access Reconnaissance Report | StEER Term |
| EERI | Earthquake Engineering Research Institute | Professional Organization |
| EEFIT | Earthquake Engineering Field Investigation Team | Professional Organization |
| EF | Enhanced Fujita Scale | Hazard Intensity Scale |
| EF | Equipment Facility | Academic Organization within NHERI |

| | | |
|--------|---|------------------------------------|
| EIFS | Exterior Insulation Finish System | Building Component |
| FAA | Federal Aviation Administration | Governmental Agency |
| FAQ | Frequently Asked Questions | Common Term |
| FAST | Field Assessment Structural Team | StEER Term |
| FEMA | Federal Emergency Management Agency | Governmental Agency |
| FIRM | Flood Insurance Rate Maps | Regulatory Product |
| GEER | Geotechnical Extreme Events Reconnaissance | Academic Organization within NHERI |
| GPS | Global Positioning System | Measurement Technology |
| GSA | Government Services Administration | Governmental Agency |
| HVAC | Heating, ventilation and air conditioning | Building System |
| HWM | High Water Mark | Intensity Measure |
| IBC | International Building Code | Code/Standard |
| ICC | International Code Council | Code Body |
| IRC | International Residential Code | Code/Standard |
| ISEEER | Interdisciplinary Science and Engineering Extreme Events Research | Academic Organization within NHERI |
| LiDAR | Light Detection and Ranging | Measurement Technology |
| MCE | Maximum Considered Earthquake | Design Terminology |
| ME&P | Mechanical, electrical and plumbing | Building System |
| MMI | Modified Mercalli Intensity | Hazard Intensity Scale |
| NBC | National Building Code | Code/Standard |
| NEER | Nearshore Extreme Event Reconnaissance | Academic Organization within NHERI |
| NFIP | National Flood Insurance Program | Government Program |
| NHERI | Natural Hazards Engineering Research Infrastructure | Academic Organization within NHERI |
| NIST | National Institute of Standards and Technology | Governmental Agency |
| NOAA | National Oceanic and Atmospheric Administration | Governmental Agency |
| NSF | National Science Foundation | Governmental Agency |

| | | |
|----------|---|-------------------------------------|
| NWS | National Weather Service | Governmental Agency |
| OSB | Oriented strand board | Construction Material |
| OSEEER | Operations and Systems Engineering Extreme Events Research | Academic Organization within NHERI |
| PEER | Pacific Earthquake Engineering Research center | Academic Organization (Earthquakes) |
| PGA | Peak Ground Acceleration | Intensity Measure |
| PHEER | Public Health Extreme Events Research | Academic Organization within NHERI |
| PVRR | Preliminary Virtual Reconnaissance Report | StEER Term |
| QC | Quality Control | Oversight process |
| RAPID | RAPID Grant | Funding Mechanism |
| RAPID-EF | RAPID Experimental Facility | Academic Organization within NHERI |
| RC | Reinforced Concrete | Building Material |
| SAR | Search and Rescue | Standard Hazards Terminology |
| SGC | Servicio Geologico Colombiano (Colombian Geological Survey) | Governmental Agency |
| SGI | Special Government Interest | FAA Process |
| SLP | Surface-Level Panoramas | Measurement Technology |
| SMS | Short Message Service | Communication Modality |
| SPC | Storm Prediction Center | Governmental Agency |
| SSEER | Social Science Extreme Events Research | Academic Organization within NHERI |
| StEER | Structural Extreme Events Reconnaissance network | Academic Organization within NHERI |
| SUMMEER | SUstainable Material Management Extreme Events Reconnaissance | Academic Organization within NHERI |
| TAS | Testing Application Standard | Technical Standard |
| UAS/V | Unmanned Aerial Survey/System/Vehicle | Measurement Technology |
| USD | US Dollar | Standard Currency |



| | | |
|------|------------------------------------|------------------------|
| USGS | United States Geological Survey | Governmental Agency |
| VAST | Virtual Assessment Structural Team | StEER Term |
| WS | Windshield Survey | Measurement Technology |

EXECUTIVE SUMMARY

On June 8, 2025, at 8:08 a.m. local time (13:08 UTC), a moment magnitude 6.4 earthquake struck near Paratebueno in the department of Cundinamarca, Colombia. The epicenter was located in the Llanos Foothills region along the eastern flank of the Colombian Andes, approximately 15 km southeast of Paratebueno. The largest recorded horizontal peak ground acceleration was 0.11 g, near Villavicencio. The 2025 Paratebueno earthquake caused widespread damage to buildings, infrastructure, and essential services across several rural communities in Cundinamarca, including Santa Cecilia, Japón, Medina, and parts of Villanueva and Barranca de Upía. These communities are characterized by limited economic resources, prevalent informal construction practices, and limited access to earthquake-resistant infrastructure.

According to the National Unit for Disaster Risk Management (UNGRD), at least 508 people were directly affected, with 362 homes damaged, 174 completely collapsed, and nearly 1,400 people displaced into temporary shelters. In Paratebueno, 134 homes collapsed and one church was damaged, while nearby Medina reported damage to homes, public institutions, and three churches. Infrastructure impacts included landslides and pavement failure along critical segments of the Villavicencio–Yopal corridor, which disrupted transportation and paralyzed local commerce. The education sector was particularly affected, with at least 27 schools destroyed. The consequences of the event highlighted the vulnerability of non-engineered structures and underscored the urgent need for resilient infrastructure in future reconstruction.

In response, StEER coordinated with colleagues in the Colombian Earthquake Engineering Research (CEER) Network to support their local response to this event, which included a self-directed survey of the impacted area on June 12, 2025. A consortium was formed between CEER, StEER, and the Earthquake Engineering Research Institute (EERI) Learning from Earthquakes (LFE) Program to author this **Joint Reconnaissance Report (JRR)**, which uses both third-party assembled virtually by CEER, StEER and EERI LFE members and CEER-field-collected data to: (1) provide an overview of the June 8, 2025 Mw 6.4 Paratebueno earthquake and its societal impacts, (2) summarize the tectonic and seismic context of this region of Colombia, (3) contextualize performance with Colombian seismic design codes and construction practices, (4) synthesize preliminary reports of damage to buildings and other infrastructure, and (5) offer recommendations for the continued study of this event by StEER and the wider engineering reconnaissance community, centered on: (i) Risk Assessment of Informal and Non-Engineered Buildings, (ii) National Risk Assessment Model for Educational Infrastructure, and (iii) Resilience of Lifelines and Rural Communities.

TABLE OF CONTENTS

| | |
|---|----|
| PREFACE | 2 |
| COPYRIGHT DISCLAIMER | 3 |
| ATTRIBUTION GUIDANCE | 4 |
| Reference to JRR Analyses, Discussions or Recommendations | 4 |
| Citing Images from this JRR | 4 |
| ACKNOWLEDGMENTS | 5 |
| COMMON TERMS & ACRONYMS | 6 |
| EXECUTIVE SUMMARY | 10 |
| TABLE OF CONTENTS | 11 |
| 1. Introduction | 13 |
| 1.1. Societal Impact | 14 |
| 1.1.1. Casualties and Injuries | 14 |
| 1.1.2. Population Exposure to Shaking | 15 |
| 1.1.3. Economic Losses | 17 |
| 1.1.4. Overall Damage and Disruption | 18 |
| 1.2. Official Response | 18 |
| 1.2.1. Emergency Mobilization and Humanitarian Aid | 18 |
| 1.2.2. Post-Earthquake Rapid Assessments | 20 |
| 1.3. Report Scope | 20 |
| 2. Hazard Characteristics | 21 |
| 2.1. Tectonic Summary | 21 |
| 2.2. Earthquake Details | 23 |
| 2.3. Recorded Ground Motions | 26 |
| 2.4. Intensity Estimates from Ground Motion Models | 29 |
| 2.4.1. PGA and Sa(1.0 s) | 30 |
| 2.4.2. PGV and Arias Intensity | 30 |
| 3. Local Codes and Construction Practices | 32 |
| 4. Building Performance | 37 |



| | | |
|------|--|----|
| 4.1. | Field Surveys | 37 |
| 4.2. | Single-family Residential Houses | 38 |
| 4.3. | Commercial Buildings | 41 |
| 4.4. | Performance of School Buildings | 43 |
| 4.5. | Religious Institutions | 48 |
| 4.6. | Site Walls | 50 |
| 5. | Infrastructure Performance | 50 |
| 5.1. | Three-span Vehicular Traffic Bridge | 51 |
| 5.2. | Single-span Vehicular Traffic Bridge | 55 |
| 5.3. | Pedestrian Bridge | 57 |
| 6. | Geotechnical Performance | 59 |
| 7. | Recommended Response Strategy | 61 |
| | TOPIC 1: Strengthen Risk Assessment of Informal and Non-Engineered Buildings | 61 |
| | TOPIC 2: National Risk Assessment Model for Educational Infrastructure | 61 |
| | TOPIC 3: Enhancing the Resilience of Lifelines and Rural Communities | 62 |
| | ESCALATION DECISION | 62 |
| | References | 63 |

1. Introduction

On June 8, 2025, at approximately 8:08 a.m. local time, a moment magnitude (Mw) 6.4 thrust-fault earthquake struck the Llanos Foothills along the eastern flank of the Colombian Andes. The Colombian Geological Survey (Servicio Geológico Colombiano [SGC], in Spanish) reported an epicenter at 4.445°N, 73.285°W (± 2.0 km), and a depth of 15.0 ± 3.0 km (SGC, 2025c). In comparison, the U.S. Geological Survey (USGS, 2025b) reported a slightly lower magnitude of Mw 6.3, with an epicenter at 4.490°N, 73.139°W (± 7.6 km), and a focal depth of 9.0 ± 1.7 km, approximately 15 km northeast of Paratebueno (Figure 1.1). Shaking from the earthquake was felt as far away as Bogota, the capital of the country, approximately 100 km from the epicenter. Within the first 48 hours following the mainshock, the SGC documented approximately 149 aftershocks. Extensive structural damage occurred near the epicenter, particularly in small towns characterized by predominantly non-engineered masonry or adobe construction, as well as poorly detailed reinforced concrete structures.

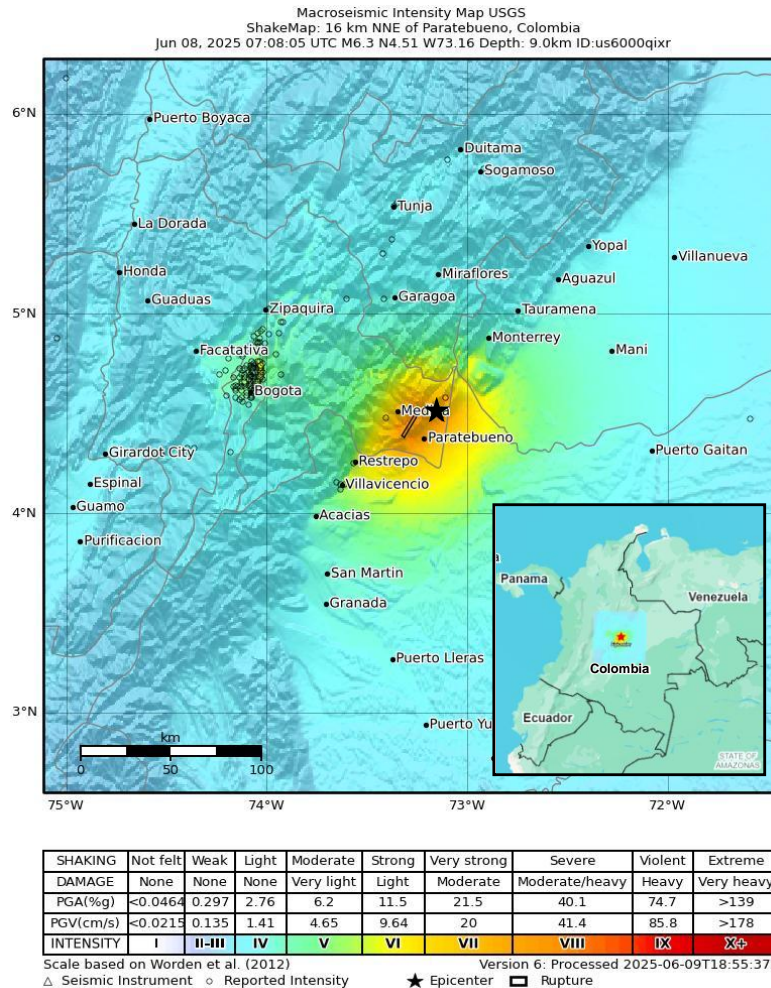


Figure 1.1. Earthquake epicenter and estimated shaking intensity in the region (Source: USGS, 2025b).

In response, StEER coordinated with colleagues in the Colombian Earthquake Engineering Research (CEER) Network to support their local response to this event, which included the deployment of a local Field Assessment Structural Team (FAST), forming a consortium between CEER, StEER, and the Earthquake Engineering Research Institute (EERI) Learning from Earthquakes (LFE) Program to develop this report.

1.1. Societal Impact

The earthquake that struck the Llanos Foothills region on June 8, 2025, had a significant societal impact, particularly on the municipalities of Paratebueno, Medina, and nearby rural communities. This section summarizes initial reports from news media and government sources regarding injuries, damage to buildings and infrastructure, and economic disruption. These reported observations are contrasted against estimates provided by PAGER, the USGS rapid-impact assessment tool (USGS, 2025c), acknowledging the limitations of applying this tool outside the United States.

1.1.1. Casualties and Injuries

The Cundinamarca Fire Department initially reported four injured people from the earthquake: two in Paratebueno and two in Medina. In Medina, the two injured people sustained trauma to their lower limbs due to the collapse of walls and façades (Presidencia de la Republica de Colombia, 2025b). As the day progressed, Colombian media reported that the number of injured individuals in these municipalities may have risen to at least 30 (El Tiempo, 2025c). In Bogotá, although the earthquake caused no direct physical injuries, one person had to be treated for an anxiety attack following the event (infobae, 2025). Neither official sources nor the media reported any casualties.

In contrast with the field reports above, PAGER estimated the probabilities of earthquake-related fatalities shortly after the event. These estimates are based on ground motion intensity estimations (USGS ShakeMap), population exposure, and vulnerability models (see Figure 1.2). The probability of earthquake-related fatalities was highest in the 1–10 deaths range (33%); there was also a 20% probability of zero fatalities.

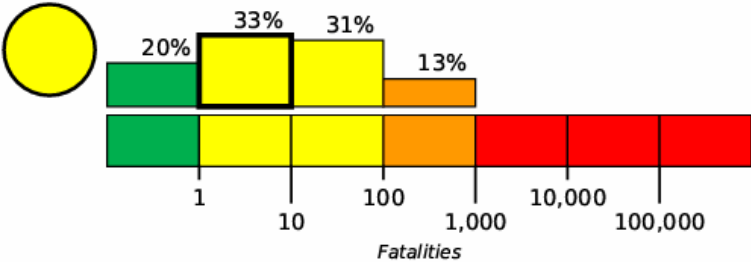


Figure 1.2. Probability distribution of number of fatalities estimated by PAGER (Source: USGS, 2025c).

While the USGS PAGER system provided a rapid probabilistic assessment of potential fatalities, its estimates did not materialize in this event, as official reports confirmed zero fatalities. This outcome underscores the usefulness of global rapid-response models for emergency preparedness as well as their limitations in capturing specific local conditions, such as the construction practices, vulnerabilities, and response capacities in countries like Colombia. As the National Seismic Risk Model of Colombia (Earthquake Spectra, 2025) continues to integrate country-specific exposure, vulnerability, and ground motion models, a valuable opportunity emerges for international collaboration. These partnerships can refine global tools like PAGER by incorporating insights from national datasets and recent events. Such efforts would help reduce epistemic uncertainties and enhance the accuracy of rapid impact forecasts worldwide, ultimately supporting more effective and proportionate disaster response strategies.

1.1.2. Population Exposure to Shaking

PAGER estimated the population exposed to ground shaking and categorized it according to Modified Mercalli Intensity (MMI) levels, along with the associated potential damage to both earthquake resistant and vulnerable structures as shown in Figure 1.3.

The population of larger urban centers (e.g., Villavicencio and Bogotá) perceived only weak to moderate shaking. Rural areas and small towns were the most affected regions (i.e., small municipalities of the Cundinamarca and Meta states). Similarly, the potential for damage to vulnerable structures was greater in regions subjected to higher intensity levels, particularly in areas characterized by a predominance of vulnerable construction (e.g., the municipalities of Medina and Paratebueno). In contrast, similar intensity levels in larger urban centers corresponded with lower damage potential due to the more widespread implementation of earthquake-resistant structures.

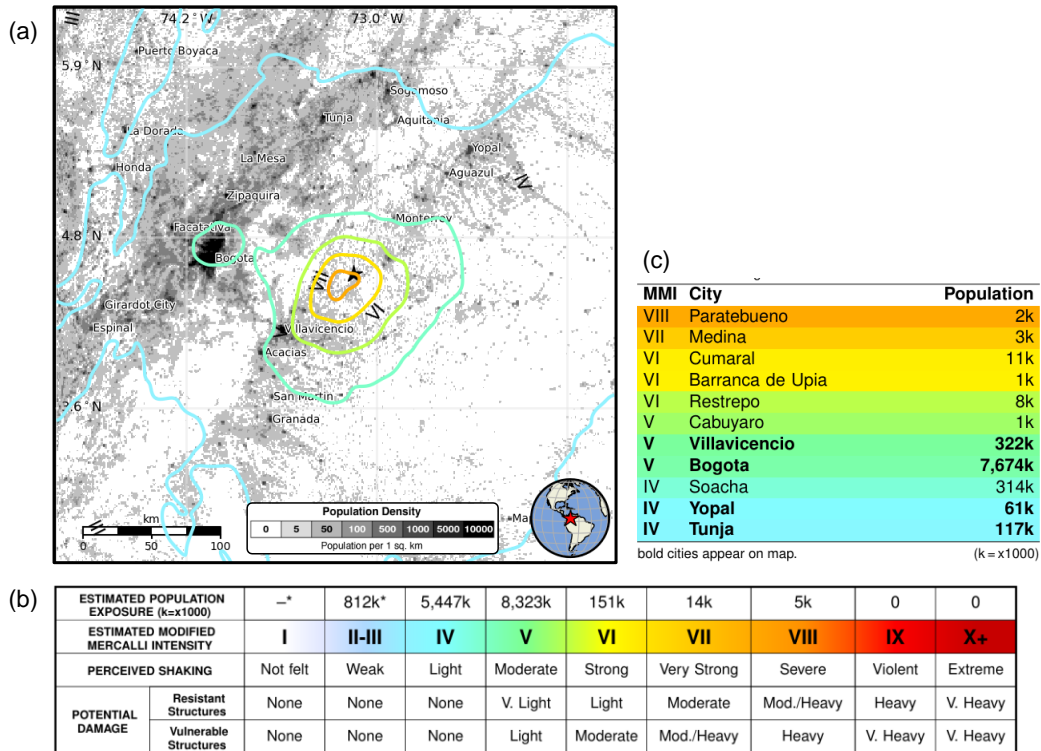


Figure 1.3. PAGER exposure estimates: (a) population density overlaid with estimated Modified Mercalli Intensity (MMI); (b) estimated population exposure and potential damage per MMI level; (c) population exposure in selected urban centers (Source: USGS, 2025c).

The SGC estimated perceived intensities on the European Macroseismic Scale (EMS-98) (Grünthal, 1998), based on more than 10,000 community-submitted Did-you-feel-it (DYF) reports (SGC, 2025c), as shown in Figure 1.4. According to these community-based estimates, municipalities including Paratebueno, Medina, and many others throughout the Departments of Cundinamarca and Meta experienced an EMS-98 intensity of VI ("Slightly Damaging"). Urban centers like Bogotá experienced less severe shaking, with an estimated EMS-98 intensity of V ("Strong"). The spatial extent of VI-level intensities reported by the community was notably wider than the area predicted by USGS PAGER estimates; however, it is important to note that the EMS-98 and MMI scales are broadly comparable but not perfectly equivalent. Furthermore, while SGC applies automatic statistical filtering to these data, this reporting may be biased due to disparities in internet access and public awareness of DYF reporting procedures between rural and urban areas.

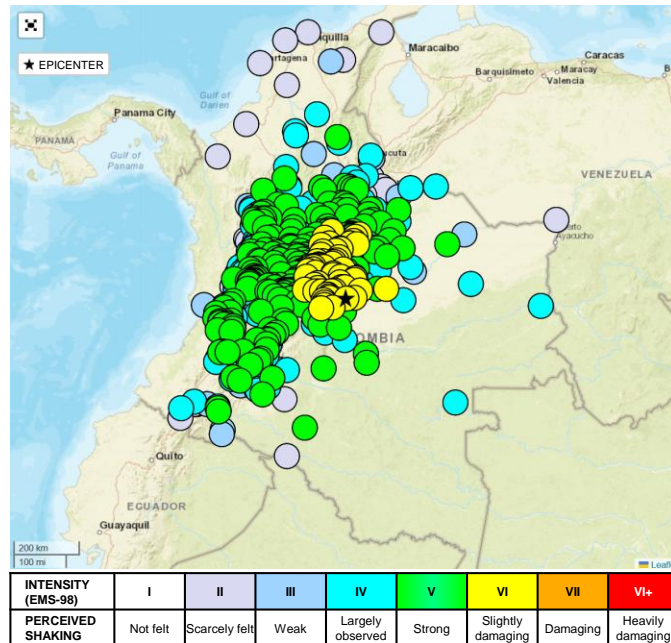


Figure 1.4. Perceived EMS-98 shaking intensities reported by the community and filtered by SGC. Colored circles refer to the aggregated intensity associated with each municipality (Source: SGC, 2025b).

1.1.3. Economic Losses

PAGER (USGS, 2025c) estimated the probabilities of economic losses across five ranges with the maximum losse estimated in the \$10-100 million range (35%), as shown in Figure 1.5. In an interview with Blu Radio, the Governor of Cundinamarca, Jorge Emilio Rey, estimated that economic losses from the earthquake were on the order of 100,000 million Colombian pesos (roughly \$24 million USD), primarily due to housing and infrastructure damage in Paratebueno and Medina (Blu Radio, 2025a). Notably, this local estimate aligns with the PAGER interval with the greatest likelihood, at 35% probability.

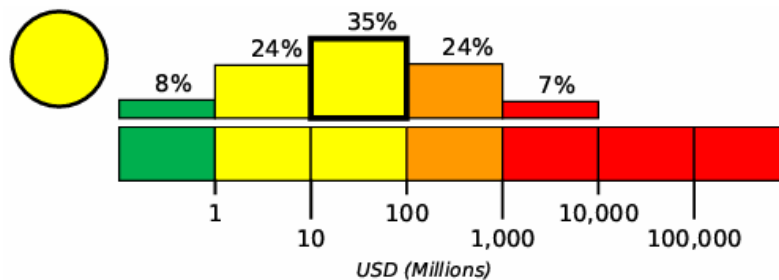


Figure 1.5. Probabilities of economic losses estimated by PAGER (Source: USGS, 2025c).

1.1.4. Overall Damage and Disruption

The earthquake caused extensive damage to buildings and infrastructure and disrupted community services. According to the National Unit for Disaster Risk Management (Unidad Nacional para la Gestión del Riesgo de Desastres [UNGRD], in Spanish), the event directly affected at least 508 people, with 362 homes damaged and 174 completely collapsed (UNGRD, 2025). In Paratebueno, 250 homes were affected, of which 134 collapsed, and one church sustained damage. In Medina, 110 homes were affected, of which 40 collapsed, three churches were damaged, and 15 public institutions reported structural impacts. A week after the earthquake, approximately 1,400 people resided in five temporary camps awaiting relocation (Caracol Radio, 2025). UNGRD continues to assess potential damage to bridges and infrastructure near the Gazamumo, Humea, and Gazaunta rivers (UNGRD, 2025).

Infrastructure damage significantly disrupted mobility and economic activity in the region. Road concessionaire Covioriente reported extensive damage to several segments of the Villavicencio–Yopal corridor, including landslides and pavement cracking across key stretches in Paratebueno, Villanueva, and Barranca de Upía (Covioriente, 2025b). Traffic restrictions and logistical interruptions resulting from the infrastructure damage paralyzed commercial activity throughout the region, devastating local businesses that serve as vital income sources for numerous families.

The educational sector also suffered significant disruption. Governor Rey reported that at least 27 schools were “*destroyed*”, forcing the suspension of classes in Paratebueno beginning on June 17, 2025. “*We have to rebuild almost 70% of the educational system of the municipality. It is a huge but urgent task,*” Rey stated, noting that the timing of the disaster, during a vacation season, likely prevented more serious consequences for school children. To address the immediate needs of the affected population, the departmental administration announced plans to implement farmers' markets, provide rent subsidies, and support entrepreneurship programs for economic recovery (Caracol Radio, 2025).

1.2. Official Response

Following the earthquake, national and departmental agencies in Colombia mobilized to deliver humanitarian assistance and assess the damage in the most affected municipalities of Paratebueno and Medina, as detailed below.

1.2.1. Emergency Mobilization and Humanitarian Aid

UNGRD activated its operational capacity and deployed a multidisciplinary response team. From the National Logistics Center, it coordinated the delivery of humanitarian aid, including 300 mats, 300 blankets, 300 hygiene kits, 18 igloo-type tents, and established an operations base to support the installation of temporary shelters (UNGRD, 2025) (see Figure 1.6). A 15,000-liter water tanker was also sent to Paratebueno to ensure water access for up to 10,000 people, due to the

disruption of essential services caused by the earthquake (Presidencia de la Republica de Colombia, 2025a). However, on the evening of June 27, a severe windstorm partially destroyed several of the temporary shelters that had been installed (Colombia.com, 2025). This secondary event further delayed the official emergency response and highlighted the vulnerability of displaced populations to compounding natural hazards in the aftermath of a significant earthquake.

Simultaneously, UNGRD deployed structural engineers and National Search and Rescue Program members to assess damage to buildings and infrastructure (UNGRD, 2025). The SGC contributed to ongoing hazard monitoring by installing seismic sensors and high-precision GPS devices throughout the region. These instruments are being used to analyze ground deformation and monitor landslide-prone areas, particularly in the village of La Europa, where an extensive mass movement event affected over 634 hectares. As a precaution, at least 80 families from this high-risk area were relocated to temporary shelters in the San Andrés 2 sports center, in the urban center of Paratebueno (Blu Radio, 2025b).

Colombian President Gustavo Petro confirmed the continued deployment of national response resources through the Presidency's press office. He emphasized the importance of interagency coordination for emergency response and early stages of recovery planning (Presidencia de la Republica de Colombia, 2025b). According to official statements, these efforts aim to restore essential services and begin the reconstruction of affected housing, public buildings, and road infrastructure (Caracol Radio, 2025).



Figure 1.6. Response in Santa Cecilia, Paratebueno (Credit: Archbold).

1.2.2. Post-Earthquake Rapid Assessments

During field visits, the FAST observed that many buildings had been marked with rapid safety assessment “placards”, following a simplified tagging system. Engineers deployed by UNGRD applied these markings to communicate the structural safety status of buildings directly to occupants and responders. The system used consisted of square symbols painted on exterior walls of the structures: an empty square indicated that the structure was safe to occupy; a square with a single diagonal line signaled restricted use; and a square with two diagonals (a full “x”) identified the building as unsafe. Figure 1.7 illustrates this marking system, showing examples of structures in Paratebueno representing each of the three safety assessment categories.



Figure 1.7. Post-earthquake safety tags observed in Paratebueno: (left) safe, (b) restricted use and unsafe (Credit: Archbold and Carrillo).

1.3. Report Scope

Deferring to CEER colleagues, StEER did not activate the traditional Level 1 response to the 2025 Paratebueno Earthquake but played a supporting role as CEER began documenting the event through a self-directed survey of the impacted area on June 12, 2025. An official [response page](#) was created on the StEER website to house any products generated by this collaboration. CEER’s access to the affected area enabled a unique form of **Joint Reconnaissance Report (JRR)**, which uses both third-party assembled virtually by CEER, StEER and EERI LFE members and CEER-field-collected data to:

1. Provide an overview of the June 8, 2025 Mw 6.4 Paratebueno earthquake and its societal impacts,
2. Summarize the tectonic and seismic context of this region of Colombia.
3. Contextualize performance with Colombian seismic design codes and construction practices.
4. Synthesize preliminary reports of damage to buildings and other infrastructure,
5. Offer recommendations for the continued study of this event by StEER and the wider engineering reconnaissance community.

2. Hazard Characteristics

2.1. Tectonic Summary

Located at the triple-junction of the Nazca, Caribbean, and South American plates, Colombia experiences oblique compression: the Nazca plate advances eastward at approximately 6 cm/yr, while the Caribbean plate drifts ESE at 1-2 cm/yr relative to the continent (Taboada et al., 2000). This far-field stress is channeled inland through a network of reverse- and strike-slip faults, foremost the larger than 900 km-long Eastern Frontal Fault System (EFFS) that defines the mountainous front of the Eastern Cordillera against the Llanos foreland and ranks among the most continuous, high-hazard structures in the nation (Survey & Paris, 2000). Recurrent seismic rupture of these thrusts, including the Quetame Mw 5.9 (2008) and Calvario Mw 6.1 (2023) earthquakes, and, most recently, the June 8, 2025 Paratebueno earthquake centered in the Llanos Foothills, East of Bogotá, illustrate how plate-driven shortening continues to generate damaging crustal events far from the subduction interface. The overall arrangement of plates, principal faults, and plate velocities is depicted in the regional tectonic map from Taboada et al. (2000) (Figure 2.1).

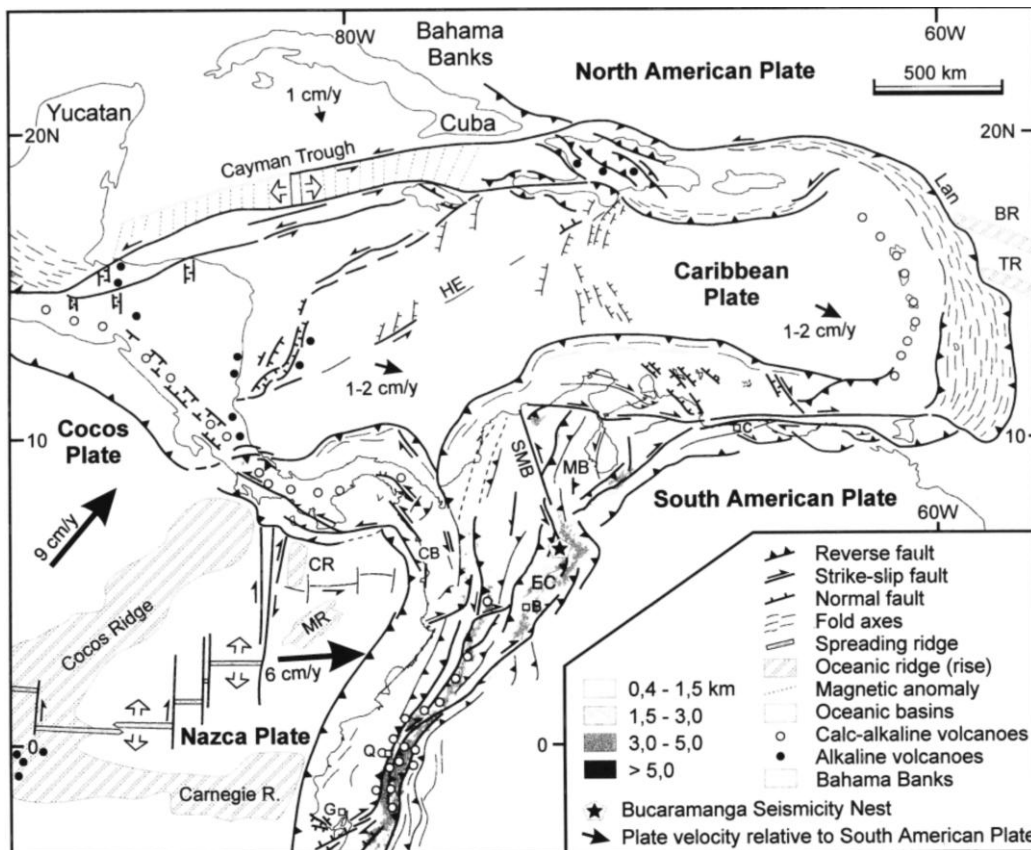


Figure 2.1. Regional tectonic framework of Colombia showing plate boundaries, principal active faults, including the Eastern Frontal Fault System, and relative plate motions (Source: Taboada et al., 2000).

Figure 2.2 plots the instrumental seismicity of the Llanos Foothills since the Colombian National Seismological Network began operations in 1993. The yellow star marks the epicenter of the June 8, 2025 earthquake near Paratebueno. The circles are sized by magnitude, while their color indicates the hypocentral depth. During this 32-year interval, the network has catalogued roughly 330 earthquakes of magnitude $M \geq 3.0$ in the foothills sector; of these, 70 events reached $M \geq 4.0$. The epicenters cluster along the mapped Piedemonte thrusts (black traces). The recorded events are shallow, with an average focal depth close to 20 km, highlighting seismogenic deformation in the upper crust. Furthermore, focal mechanisms routinely released by the SGC for this region indicate that most events aligned with the foothill faults exhibit reverse faulting, which is consistent with ongoing crustal shortening accommodated by the EFFFs.

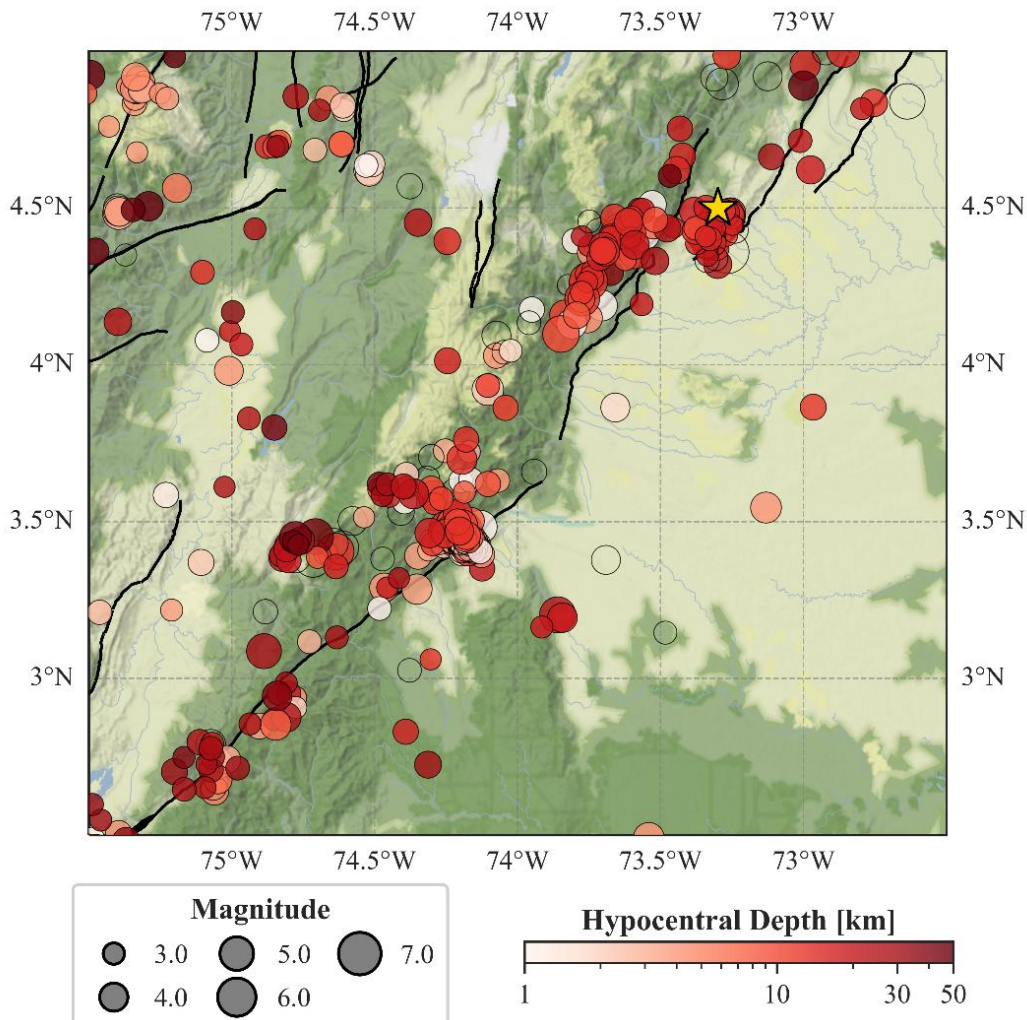


Figure 2.2. Instrumental seismicity ($M \geq 3.0$, 1993-2025) in the Llanos Foothills: symbol size scales with magnitude, color indicates hypocentral depth, and black traces mark active faults along the Andean front.

2.2. Earthquake Details

At 08:08 a.m. local time (13:08 UTC) on June 8, 2025, the SGC recorded a moment magnitude M_w 6.4 thrust-fault earthquake along the Llanos Foothills, with epicentral coordinates of 4.445° N, 73.285° W (± 2 km) and a focal depth of 15 km (± 3 km). The event was assigned a maximum instrumental intensity of VIII on the Worden et al. (2012) scale. Within the first 48 hours, the SGC documented approximately 149 aftershocks. Later that morning, a preliminary bulletin (Arteta & Caballero, 2025), released at 11:00 a.m. local time (16:00 UTC), summarized strong-motion observations and presented the ground-motion map shown in Figure 2.3.

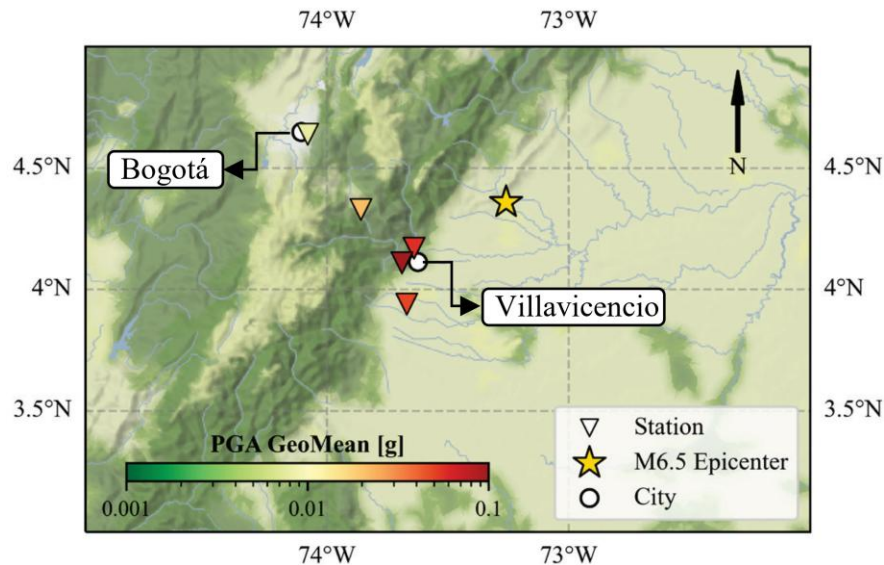


Figure 2.3. Preliminary PGA map (geometric mean) for the June 8, 2025 Paratebueno earthquake; colored triangles show strong-motion stations (Source: Arteta & Caballero, 2025).

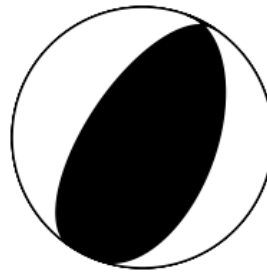
The moment-tensor solution released by the SGC (SGC, 2025c) portrays the main shock as a shallow reverse event. Its hypocenter is located at 4.5° N, 73.3° W at a 10 km depth, with a seismic moment of 4.85×10^{18} N.m corresponding to M_w 6.4. The two nodal planes (Table 2.1) indicate either a northeast-striking, moderately dipping fault (strike 20° , dip 39° , rake 79°) or a southwest-striking, steeper structure (strike 214° , dip 52° , rake 99°); both geometries are consistent with thrusting on the west-dipping Piedemonte faults. The principal-axis orientations (Table 2.2) show a nearly vertical P-axis (plunge 81° , azimuth 165°) and shallow T- and N-axes, confirming a compressional regime with horizontal NE–SW shortening. These parameters yield the beach-ball diagram presented in Figure 2.4, whose shaded compressional quadrants illustrate the dominant reverse-faulting mechanism characteristic of the EDFS.

Table 2.1. Nodal planes by SGC (2025c).

| Plane | Strike | Dip | Rake |
|-------|--------|-----|------|
| NP1 | 20° | 39° | 79° |
| NP2 | 214° | 52° | 99° |

Table 2.2. Principal Axes by SGC (2025c).

| Axis | Plunge | Azimuth |
|------|--------|---------|
| P | 81° | 165° |
| T | 6° | -63° |
| N | 6° | 28° |


Figure 2.4. Fault plane solution (Source: SGC, 2025c).

The instrumental shake map (processed by the SGC at 13:08 UTC) indicates that the area immediately adjacent to the epicenter reached an instrumental intensity of VIII on the Worden et al. (2012) scale, signifying very strong shaking (see Figure 2.5). The PGA map (Figure 2.6a) reveals peak values of roughly 0.5 g within about 10 km radius around Paratebueno and Cumaral, with gradients dropping off rapidly toward the foothills and the eastern plains. The PGV map (Figure 2.6b) is consistent with this pattern, recording peaks of about 50 cm/s in the same area. In contrast, the 10 cm/s and 5 cm/s PGV contours extend over Villavicencio and part of the Bogotá savannah, respectively.

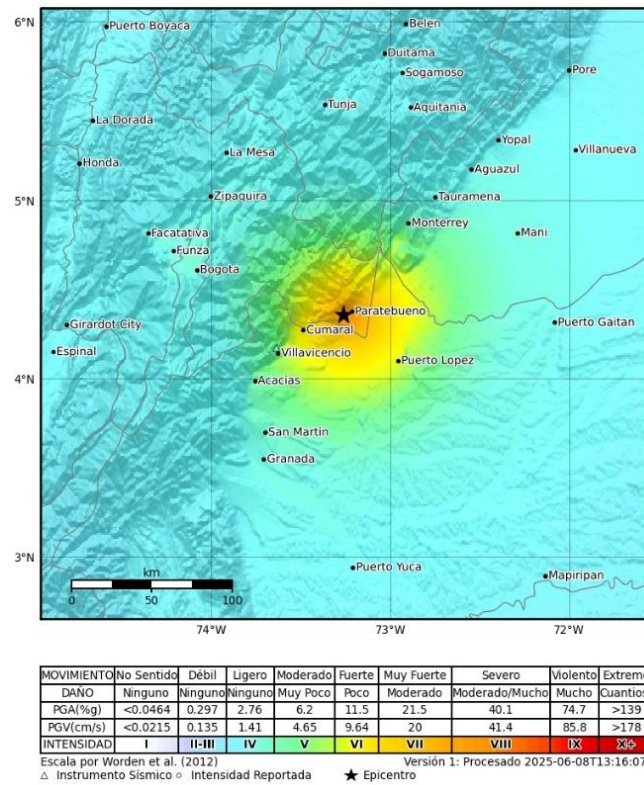


Figure 2.5. Intensities estimated from shake map (Source: SGC, 2025c).

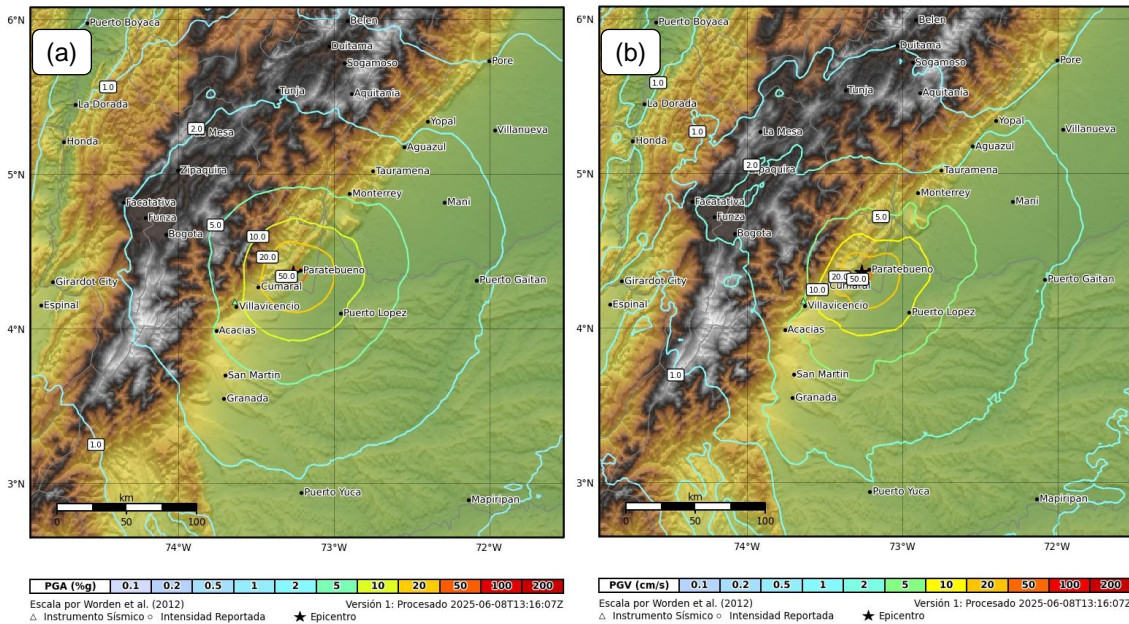


Figure 2.6. Shake map ground-motion fields for the 8 June 2025 Paratebueno earthquake: (a) peak ground acceleration (PGA, %g) and (b) peak ground velocity (PGV, cm/s). (Source: SGC, 2025c).

2.3. Recorded Ground Motions

The National Seismic Network, operated by SGC, recorded the event across 66 accelerograph stations, with complete acceleration time series successfully retrieved from 64 stations. Figure 2.7 presents 5 %-damped response spectra (for the EW, NS and Z components) from the four stations closest to the epicenter as listed in Table 2.3: Villavicencio (VIL and CVIL1), Acacias (ACH1), and Bogotá (BOG). According to Arteta et al. (2023), stations VIL, ACH1, and BOG are classified as soft-soil sites, whereas CVIL1 is located on rock. VIL exhibits intermediate-period amplification, reaching ~ 0.50 g at $T \approx 0.9$ s, while BOG shows more modest amplification (~ 0.13 g) at $T \approx 2.3$ s. In contrast, ACH1 peaks at short periods, with maximum spectral acceleration below $T \approx 0.4$ s, and CVIL1 (the rock site) displays a relatively flat spectrum decaying rapidly beyond $T \approx 0.5$ s.

Table 2.3 reports PGA and selected 5 %-damped spectral ordinates (S_a) for the EW, NS, and Z components at the ten stations nearest the Mw 6.4 epicenter ($R_{rup} \leq 140$ km). The final two columns of the table report the maximum horizontal spectral acceleration ($S_{a_{max}}$) and the period at which it occurs (T_{max}) for each station. Figure 2.8 synthesizes the spatial distribution of horizontal-geomean ground motions. Panel (a) illustrates the steep attenuation of PGA with distance from the epicenter: Villavicencio (VIL) recorded 0.11 g, whereas fore-arc stations west of the volcanic front (e.g., Cali, Buenaventura, Tumaco) registered values below 0.02 g. Panel (b) shows a comparable pattern for $S_a(1.0s)$, with intermediate-period demands concentrated in the Llanos Foothills and decaying rapidly toward the fore-arc.

These observations confirm that the strongest shaking from the June 8, 2025 earthquake was concentrated in the back-arc Piedemonte, while motions in the fore-arc remained weak. Notably, despite lying nearly 100 km farther from the epicenter, the Bogotá station, classified as a soft-soil site by Arteta et al. (2023) based on its predominant period, recorded $S_a(1.0s)$ values comparable to those at the Villavicencio rock site CVIL1, underscoring the influence of local site effects superimposed on regional attenuation trends.

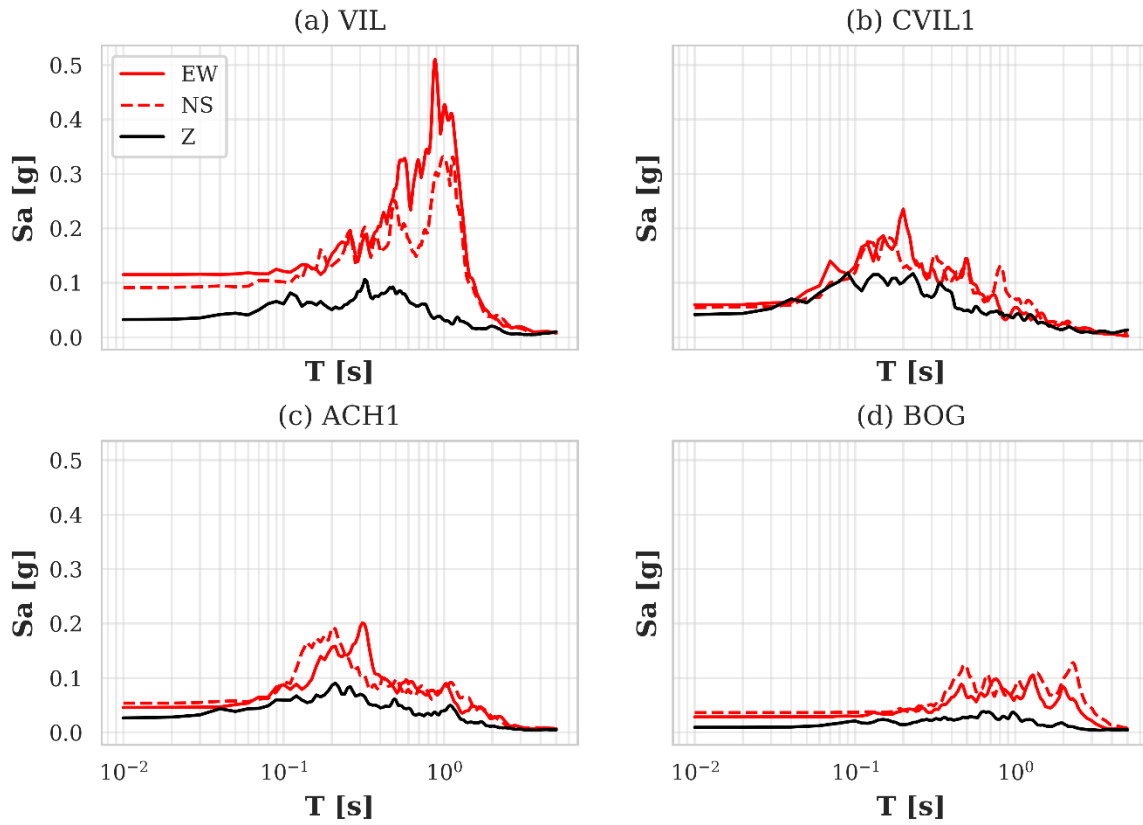


Figure 2.7. 5 %-damped response spectra (S_a) for the EW (solid red), NS (dashed red) and vertical (black) components recorded at (a) Villavicencio - VIL, (b) Villavicencio - CVIL1, (c) Acacías - ACH1 and (d) Bogotá – BOG.

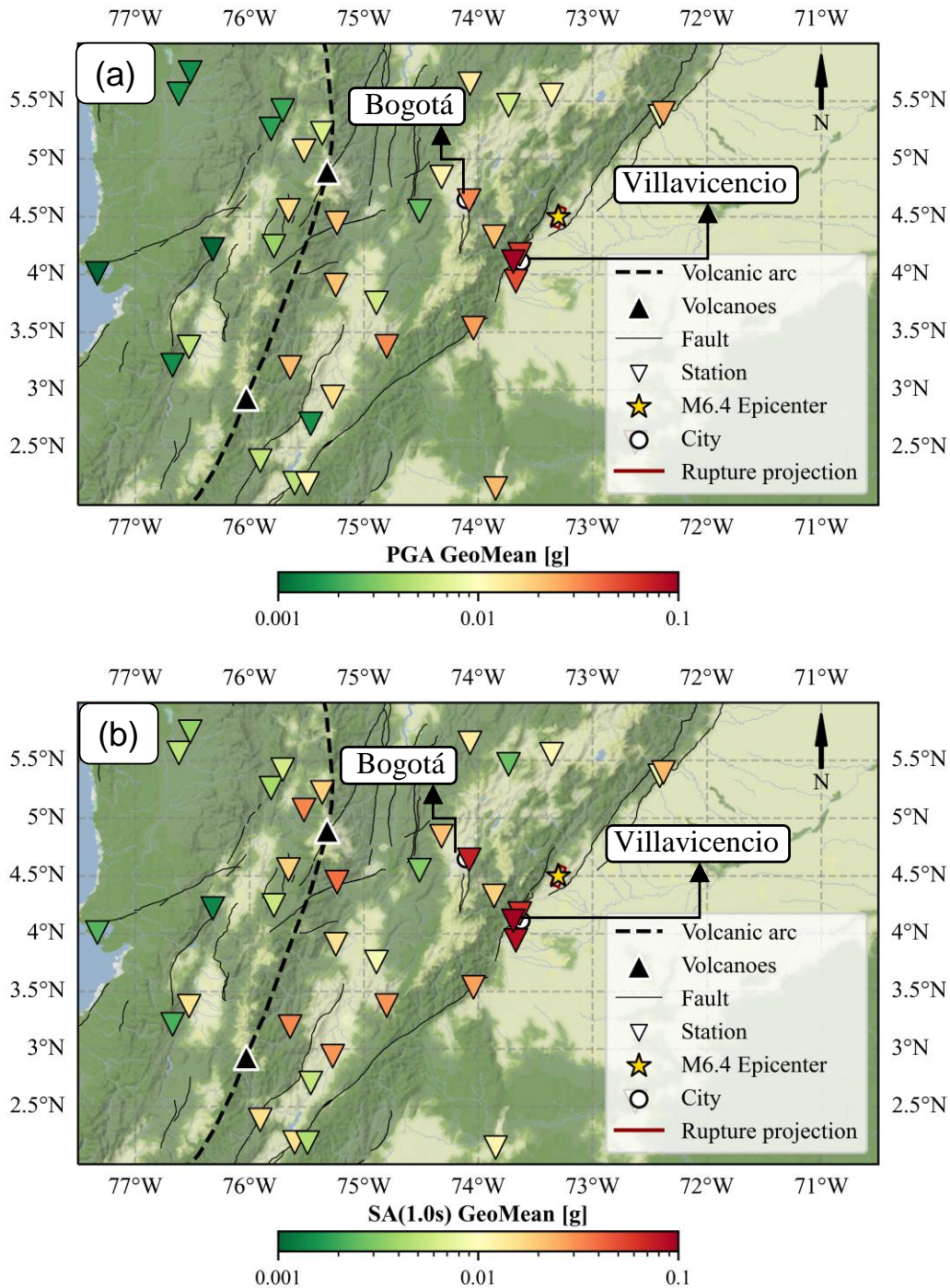


Figure 2.8. Recorded ground-motion field for the June 8, 2025 Paratebueno earthquake: (a) PGA and (b) 1.0 s spectral acceleration ($S_a(1.0\text{ s})$), both plotted as the geometric mean of the horizontal components.

Table 2.3. Three-component PGA and selected spectral ordinates for the ten stations nearest the Mw 6.4 Paratebueno epicenter.

| Station | Chanel | PGA [g] | T=0.1 [g] | T=0.3 [g] | T=0.5 [g] | T=1.0 [g] | T=3.0 [g] | Sa _{max} [g] | T _{max} [s] |
|-------------------------------------|--------|---------|-----------|-----------|-----------|-----------|-----------|-----------------------|----------------------|
| CVIL1 R _{rup} =42.4 km | EW | 0.060 | 0.130 | 0.128 | 0.144 | 0.055 | 0.010 | 0.235 | 0.2 |
| | NS | 0.055 | 0.119 | 0.133 | 0.125 | 0.070 | 0.010 | 0.184 | 0.16 |
| | Z | 0.042 | 0.096 | 0.073 | 0.050 | 0.041 | 0.006 | 0.118 | 0.09 |
| VIL R _{rup} =55.5 km | EW | 0.115 | 0.121 | 0.156 | 0.273 | 0.425 | 0.004 | 0.510 | 0.88 |
| | NS | 0.091 | 0.102 | 0.169 | 0.248 | 0.331 | 0.012 | 0.332 | 0.99 |
| | Z | 0.033 | 0.061 | 0.084 | 0.080 | 0.031 | 0.001 | 0.106 | 0.32 |
| ACH1 R _{rup} =64.2 km | EW | 0.046 | 0.088 | 0.194 | 0.077 | 0.086 | 0.001 | 0.201 | 0.31 |
| | NS | 0.054 | 0.093 | 0.105 | 0.097 | 0.085 | 0.001 | 0.193 | 0.2 |
| | Z | 0.027 | 0.059 | 0.070 | 0.060 | 0.040 | 0.001 | 0.091 | 0.21 |
| CQUET R _{rup} =55.5 km | EW | 0.018 | 0.039 | 0.033 | 0.026 | 0.017 | 0.001 | 0.061 | 0.14 |
| | NS | 0.025 | 0.057 | 0.052 | 0.049 | 0.019 | 0.002 | 0.109 | 0.15 |
| | Z | 0.020 | 0.036 | 0.054 | 0.038 | 0.011 | 0.001 | 0.057 | 0.29 |
| BOG R _{rup} =83.0 km | EW | 0.029 | 0.030 | 0.037 | 0.064 | 0.064 | 0.006 | 0.106 | 1.28 |
| | NS | 0.036 | 0.037 | 0.051 | 0.118 | 0.084 | 0.004 | 0.128 | 2.29 |
| | Z | 0.010 | 0.021 | 0.022 | 0.027 | 0.034 | 0.002 | 0.038 | 0.63 |
| CLEJA R _{rup} =123.9 km | EW | 0.025 | 0.058 | 0.050 | 0.046 | 0.028 | 0.021 | 0.066 | 0.33 |
| | NS | 0.030 | 0.069 | 0.080 | 0.047 | 0.026 | 0.044 | 0.097 | 0.14 |
| | Z | 0.013 | 0.063 | 0.033 | 0.022 | 0.020 | 0.005 | 0.063 | 0.1 |
| ROSC R _{rup} =108.4 km | EW | 0.013 | 0.013 | 0.030 | 0.035 | 0.020 | 0.004 | 0.054 | 0.64 |
| | NS | 0.011 | 0.012 | 0.037 | 0.043 | 0.023 | 0.003 | 0.045 | 0.49 |
| | Z | 0.005 | 0.005 | 0.015 | 0.015 | 0.013 | 0.001 | 0.016 | 0.33 |
| CTUN3 R _{rup} =106.0 km | EW | 0.013 | 0.017 | 0.031 | 0.032 | 0.014 | 0.000 | 0.043 | 0.46 |
| | NS | 0.012 | 0.015 | 0.031 | 0.028 | 0.009 | 0.000 | 0.045 | 0.45 |
| | Z | 0.005 | 0.010 | 0.010 | 0.011 | 0.013 | 0.001 | 0.016 | 0.17 |
| CFQNE R _{rup} =133.9 km | EW | 0.005 | 0.006 | 0.010 | 0.014 | 0.002 | 0.003 | 0.019 | 0.38 |
| | NS | 0.007 | 0.007 | 0.021 | 0.021 | 0.004 | 0.001 | 0.022 | 0.53 |
| | Z | 0.002 | 0.002 | 0.005 | 0.005 | 0.002 | 0.002 | 0.006 | 0.4 |
| CANAP R _{rup} =140.6 km | EW | 0.003 | 0.003 | 0.007 | 0.010 | 0.004 | 0.000 | 0.012 | 0.75 |
| | NS | 0.002 | 0.003 | 0.004 | 0.007 | 0.003 | 0.000 | 0.007 | 0.61 |
| | Z | 0.001 | 0.002 | 0.002 | 0.003 | 0.002 | 0.000 | 0.004 | 0.83 |

2.4. Intensity Estimates from Ground Motion Models

Recent advances in regional ground motion modeling in Colombia have significantly improved the characterization of seismic hazard across the country. Since 2021, collaborative research between Universidad del Norte (Uninorte) and SGC has produced four major ground motion models (GMMs), including: two for subduction earthquakes (Arteta et al., 2021), a crustal earthquake model directly relevant to this study (Arteta et al., 2023), and a dedicated model for the Bucaramanga Seismic Nest (Pajaro et al., 2024). These models are complemented by site amplification models developed by Mercado et al. (2023, 2004), which enhance understanding of local site response across Colombia. Most recently, Pajaro (2024) introduced additional crustal

GMMs for Arias Intensity (AI) and Peak Ground Velocity (PGV). Collectively, this suite of regional GMMs provides a robust framework for benchmarking recorded ground motions.

In this section, ground-motion recorded data from the June 8, 2025 earthquake are compared against estimates from the regional models, focusing on four intensity measures: PGA, Sa(1.0 s), PGV, and AI. The results are shown in Figure 2.9, distinguishing ground motion records by site condition (soil, rock) and location of the recording station relative to the volcanic front (fore-arc to the east, back-arc to the west). The GMMs of interest incorporate site effects using a classification approach based on the predominant period of the station, T_n . For this comparison, soil-site estimates were generated using the s4 class, which represents medium soils with $0.4 \leq T_n \leq 0.8$ s and approximately $200 \text{ m/s} \leq V_{S30} \leq 300 \text{ m/s}$.

2.4.1. PGA and Sa(1.0 s)

Figure 2.9(a) and (b) compare the recorded PGA and Sa (1.0 s, 5%-damped) values against estimates from the crustal GMM by Arteta et al. (2023). Median estimates and $\pm 1\sigma$ variability (16th–84th percentile) are shown for both soil and rock sites. In general, the observations fall within the model’s estimation bands. Estimates for rock-site PGA values matched observations well, with all recorded values falling within the $\pm 1\sigma$ range. In contrast, PGA values at several soil-site stations fell below the 16th percentile, particularly those located more than 100 km away from the source. These discrepancies likely resulted from a site classification mismatch: while soil-site GMM estimates were calibrated for s4 soil sites, the underpredicted stations are on stiffer s3 ground ($300 \text{ m/s} \leq V_{S30} \leq 600 \text{ m/s}$). Additionally, back-arc stations exhibited consistently lower PGA levels relative to the rock-site median, indicating additional attenuation across the volcanic arc as described by Arteta et al. (2023). For Sa(1.0 s), the scatter broadened: multiple soil-site stations lay outside the 16th–84th percentile envelope, and the model clearly underestimated the Sa(1.0 s) values measured at the nearest soil station.

2.4.2. PGV and Arias Intensity

Figure 2.9(c) and (d) extend the comparison to PGV and AI using the more recent GMMs developed by Pajaro (2024). Notably, the Paratebueno event is the first time these GMMs are tested against new data. For PGV at soil sites, observations scattered symmetrically about the median estimate, with most data points lying within the $\pm 1\sigma$ band. The four soil-site stations that fell outside this band all correspond to stiffer s3 soil sites (Arteta et al., 2023). Furthermore, back-arc soil-site stations located beyond 200 km tended to fall below the $\pm 1\sigma$ band, reinforcing the expected pattern of increased attenuation across the arc. In contrast, PGV observations at rock sites aligned well with the rock-site median out to approximately 150 km, but two distant back-arc stations beyond this distance fell below the rock-site median estimate.

For Arias Intensity, the regional model reproduced the ground motion data well up to intermediate distances. The model's performance, however, varied by site and location. For soil sites, several observations beyond approximately 400 km fell below the 16th percentile, suggesting that long-path attenuation may be stronger than what the s4-based model accounted for. Rock sites, in contrast, followed the rock-site median closely, with only two data traces falling outside the $\pm 1\sigma$ range. Among all stations, back-arc stations exhibited the most rapid decay in AI, consistent with the attenuation observed for PGA, Sa and PGV after seismic waves crossed the volcanic arc.

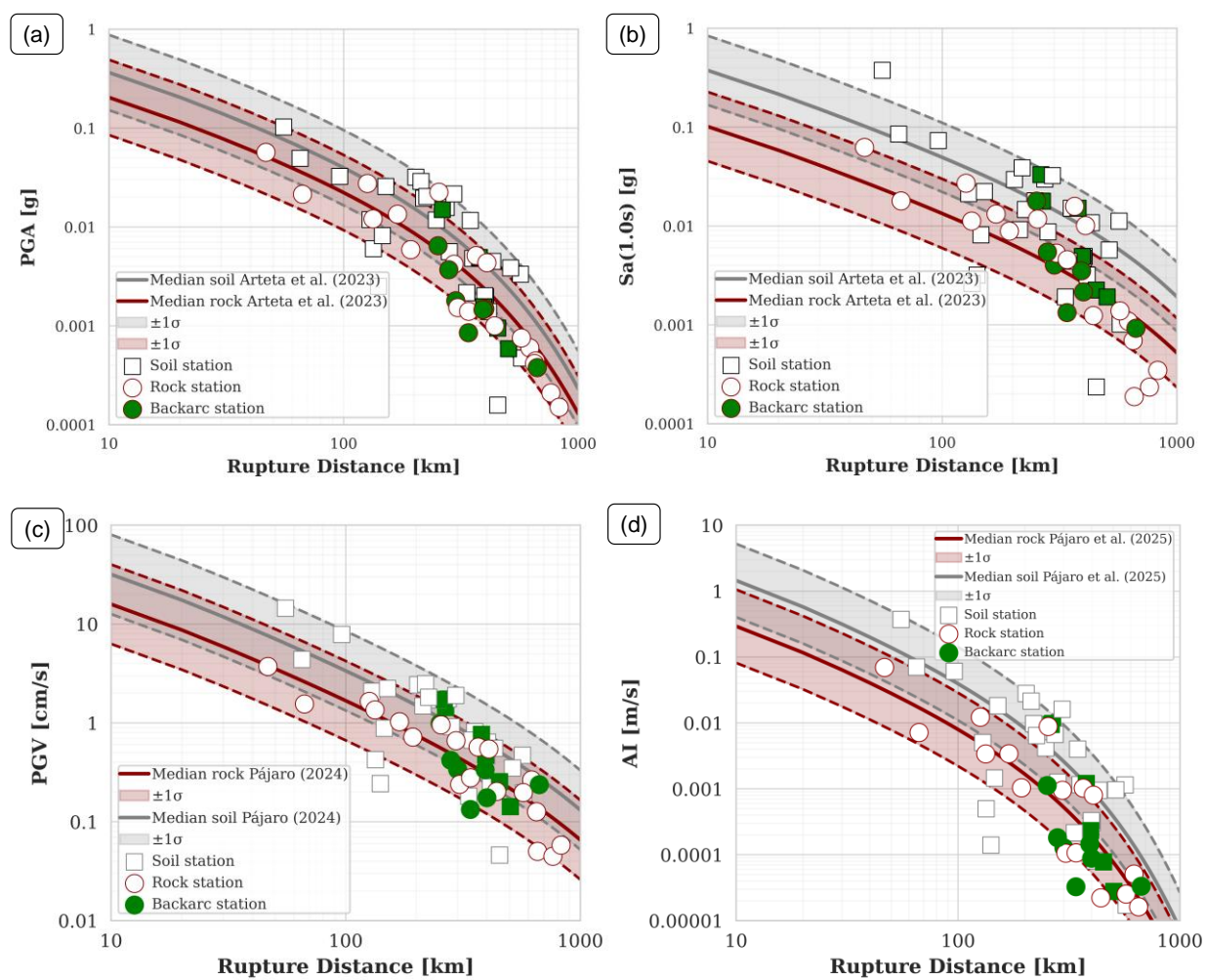


Figure 2.9. Distance-attenuation plots for the June 8, 2025 Paratebueno earthquake: (a) PGA and (b) Sa (1 s, $\xi = 5\%$) compared with soil (black) and rock (red) branches of Arteta et al. (2023); (c) PGV and (d) AI compared against Pájaro et al. (2024). Shaded bands denote $\pm 1\sigma$. Squares = soil stations, open circles = rock stations, green circles = back-arc stations.

3. Local Codes and Construction Practices

The first Colombian seismic design code was published in 1984 by the Colombian Association for Earthquake Engineering (AIS) (AIS, 1984). This code was an institutional response for improving the design and construction practices in the country. Its development was a direct result of the M5.6 Popayán Earthquake (March 31, 1983), which caused at least 200 fatalities in Popayán and 50 more in the Cauca region (Sarabia Gómez et al., 2022). The seismic map developed by AIS (1984) was the basis of this code. In 1996, the AIS published updated hazard maps (AIS, 1996) that served as the input for the NSR-98 seismic code (AIS, 1998). The current code NSR-10 (Ministerio de Ambiente, Vivienda y Desarrollo Territorial, 2010), was similarly developed from the hazard maps published by AIS (2009). This hazard study utilized the Ground Motion Model (GMM) by Campbell (1997) for crustal earthquakes, which showed lower residuals against Colombian ground-motion data.

Colombian codes use a conventional force-based/displacement-check approach. The design basis earthquake is typically an event with a 475-year return period as recommended by the former UBC-97 code. The current NSR-10 code defines three seismic hazard levels based on the maximum between the dimensionless coefficients that represent expected effective peak horizontal acceleration for design in the bedrock, A_A and the effective peak horizontal velocity for design (in bedrock) A_V . The hazard levels are defined as follows:

- Low: $\max(A_A, A_V) \leq 0.10$,
- Medium: $0.15 \leq \max(A_A, A_V) \leq 0.20$, and
- High: $0.25 \leq \max(A_A, A_V) \leq 0.50$.

The epicenter zone in Paratebueno is classified as a high-hazard zone, with $A_A=0.25$ and $A_V=0.30$. For site-specific analysis, in this case focused on the five stations closest to the epicenter, V_{S30} values were inferred using the equation suggested by Arteta et al. (2023). The predominant period of each station T_n was gathered from Mercado et al. (2023):

$$\log_{10}(V_{S30}) = 2.2 + 0.63 \log_{10}\left(\frac{1}{T_n}\right), \quad T_n < 1.09 \text{ s} \quad (3.1)$$

for $T_n \geq 1.09 \text{ s}$, $V_{S30} = 150$. The soil types specified in the NSR-10 code defined by V_{S30} were used to compute the design spectra using amplification factors for acceleration F_a and velocity F_v . Figure 3.1 illustrates the design spectra; Figures 3.2 to 3.6 show the response spectra of the two horizontal components at the five stations nearest to the epicenter based on the input parameters in Table 3.1. I is the coefficient of importance and is equal to 1.0 for residential buildings; Figures 3.2 to 3.6 were generated with $I=1.0$.

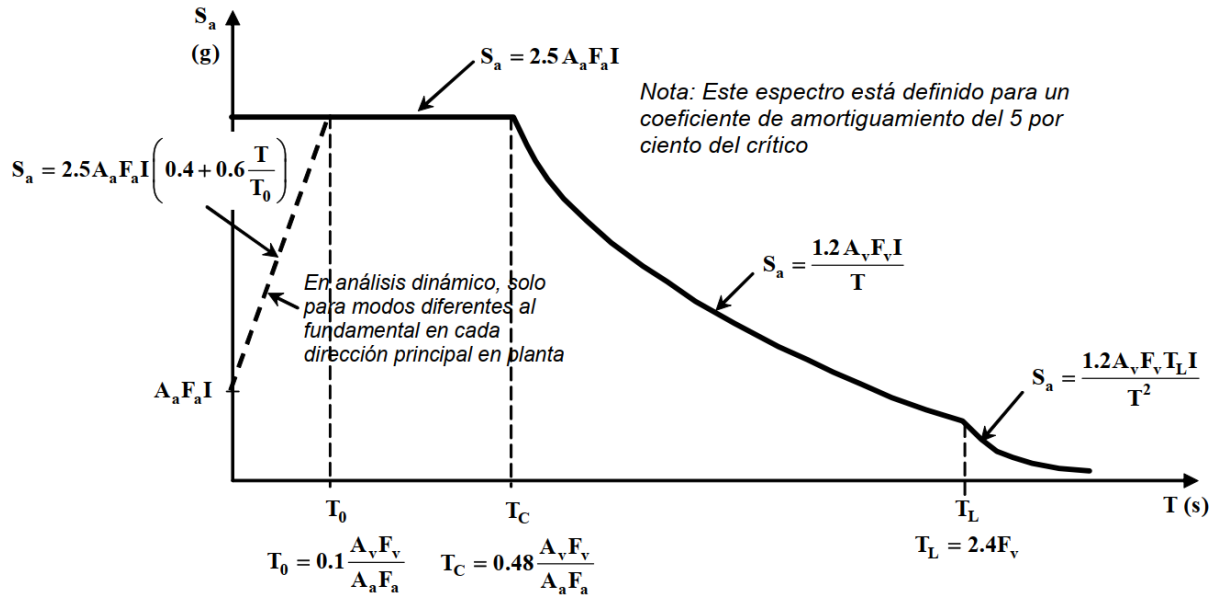


Figure 3.1. The NSR-10 definition of design spectra. The comment related to the dashed line stands for dynamic analysis, for modes other than the fundamental, in each principal direction in plan. The note clarifies that the spectra is defined for 5% of the critical damping (Source: section A (Fig. A.2.6-1) of NSR-10 document from Ministerio de Ambiente, Vivienda y Desarrollo Territorial, 2010).

Table 3.1. Input parameters for stations used to plot the design spectra according to the NSR-10 requirements. Note that V_{S30} for station BOG is the only one available by measurement.

| Station | V_{S30} (m/s) | Soil type (NSR-10) | A_A | A_V | F_a | F_v | Hazard level |
|---------|-----------------|--------------------|-------|-------|-------|-------|--------------|
| CVIL1 | 353.42 | D (medium soil) | 0.25 | 0.30 | 1.3 | 1.8 | High |
| VIL | 158.49 | E (soft soil) | 0.25 | 0.30 | 1.4 | 2.3 | High |
| ACH1 | 182.41 | D (medium soil) | 0.30 | 0.30 | 1.3 | 1.8 | High |
| CQUET | 338.39 | D (medium soil) | 0.25 | 0.25 | 1.3 | 1.8 | High |
| BOG | 110 (measured) | E (soft soil) | 0.15 | 0.20 | 2.1 | 3.2 | Medium |

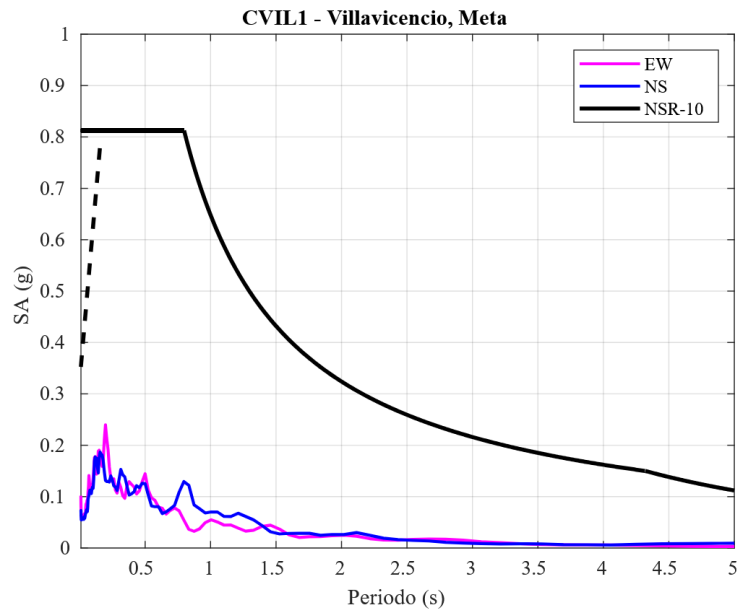


Figure 3.2. Response spectra for horizontal components EW and NS in station CVIL1 located in Villavicencio, Meta against design spectra for the 475-year return period according to NSR-10 code.

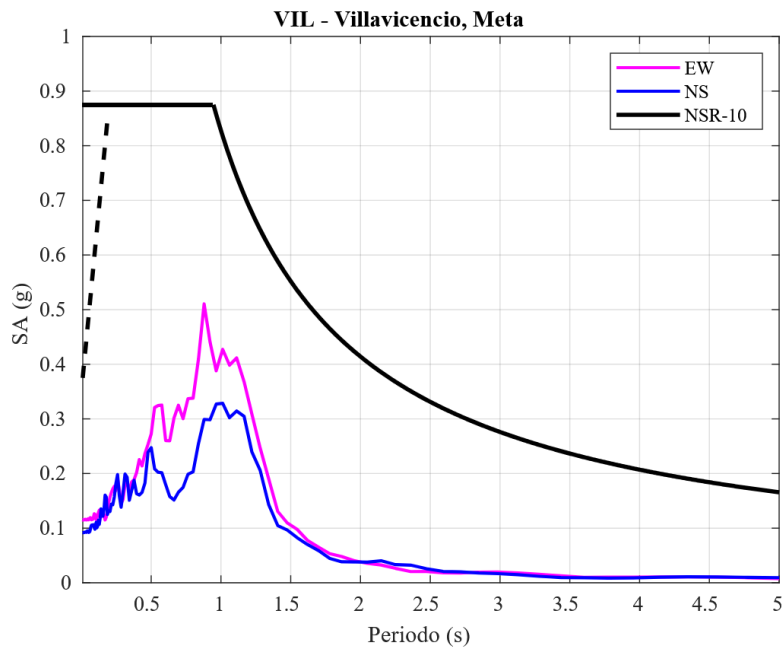


Figure 3.3. Response spectra for horizontal components EW and NS in station VIL located in Villavicencio, Meta against design spectra for the 475-year return period according to NSR-10 code.

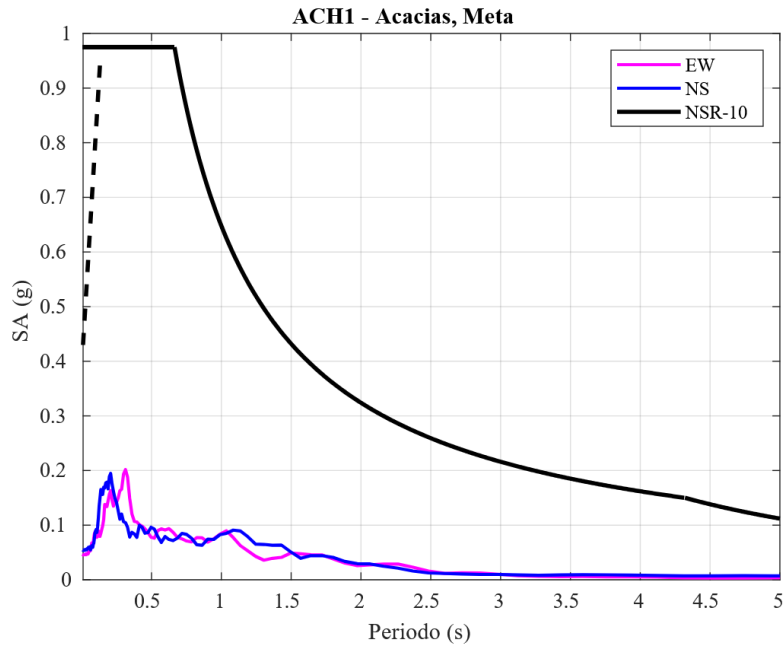


Figure 3.4. Response spectra for horizontal components EW and NS in station ACH1 located in Acacias, Meta against design spectra for the 475-year return period according to NSR-10 code.

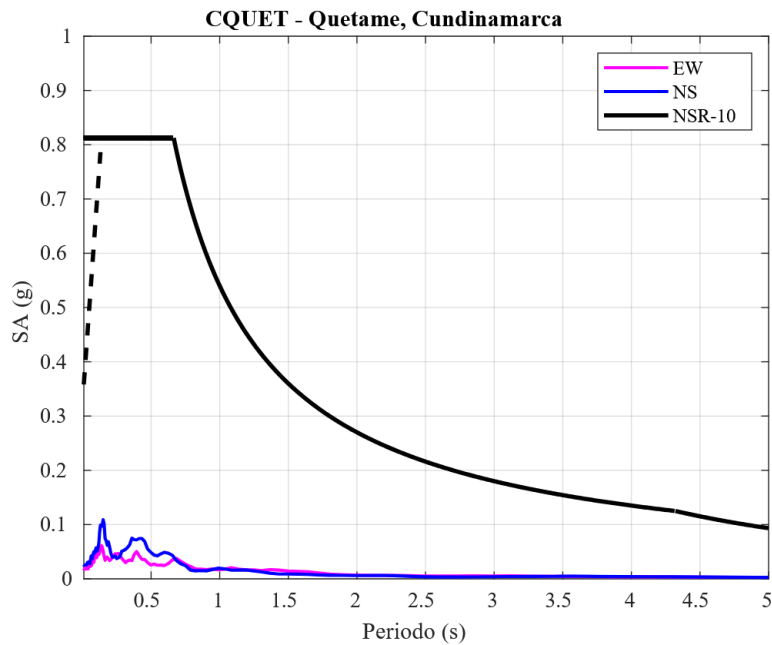


Figure 3.5. Response spectra for horizontal components EW and NS in station CQUET located in Quetame, Cundinamarca against design spectra for the 475-year return period according to NSR-10 code.

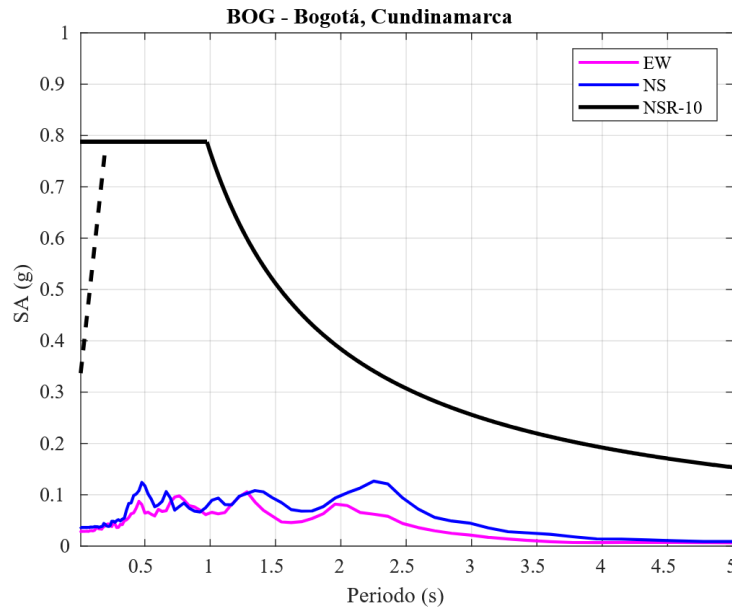


Figure 3.6. Response spectra for horizontal components EW and NS in station BOG located in Bogotá, Cundinamarca against design spectra for the 475-year return period according to NSR-10 code.

The allowable drifts prescribed by the latest seismic design code, NSR-10, are very different from the values prescribed in the previous versions (CCCSR-84 and NSR-98). When compared to the 2.0% or 2.5% drift limits for the collapse prevention limit state in ASCE 7, the 1.0% drift limit in NSR-10 is more related to a serviceability than a collapse prevention limit state, even though the text within the code refers to it as a collapse prevention limit state. The 1984 seismic code specified a drift limit of 1.5% and this value was reduced to 1.0% in NSR-98.

The reason for this reduction was to prevent nonstructural damage and to encourage the use of shear walls. Protecting nonstructural elements is a critical issue in a country with limited economic resources like Colombia, as pointed out in previous studies. The core of the problem is the challenge of preventing nonstructural damage while designing a ductile structure under the same seismic scenario. In general, the serviceability limit state seems coherent with the drift limits prescribed by the code, while the collapse prevention limit state seems coherent with reduction factors R suggested by the code (Carrillo et al., 2013).

4. Building Performance

The 2025 Paratebueno earthquake caused significant damage to buildings in the epicentral region, with pronounced impacts in small towns and rural communities such as Santa Cecilia, Japón, and Medina. The observed damage patterns reflect the diversity of construction typologies in the region, ranging from non-engineered masonry and informal construction to reinforced concrete frame structures with varying levels of seismic detailing.

This section summarizes the performance of buildings by occupancy and geographic location, focusing on the structural and non-structural damage documented during field reconnaissance. The CEER FAST conducted field surveys in the days following the event, recording common failure mechanisms such as out-of-plane wall collapses, soft-story behavior, and partial or total structural collapse in vulnerable typologies. In contrast, engineered structures that incorporated better construction practices, such as confined masonry and well-detailed reinforced concrete frames, generally demonstrated more favorable seismic performance.

However, damage to residential housing, schools, and religious institutions highlights the urgent need for targeted retrofitting efforts and stricter enforcement of seismic design standards, particularly for essential community infrastructure. The case studies presented in this section illustrate typical failure modes and emphasize the critical role of construction quality and structural configuration in determining building response during seismic events.

4.1. Field Surveys

The CEER FAST conducted preliminary reconnaissance on June 12, 2025, four days after the event. The effort was led by Jorge Archbold of Universidad del Norte, in collaboration with Julian Carrillo from Universidad Militar Nueva Granada. The survey aimed to collect information on the damage patterns around ground motion stations when possible, the behavior of masonry structures and reinforced concrete structures, as well as the disaster response on the ground.

GIS was used to aid post-survey analysis, merging building locations with other relevant data such as soil conditions, ground motion intensity, etc. Figure 4.1 shows the surveyed area in the epicentral region relative to the stations that recorded the event.

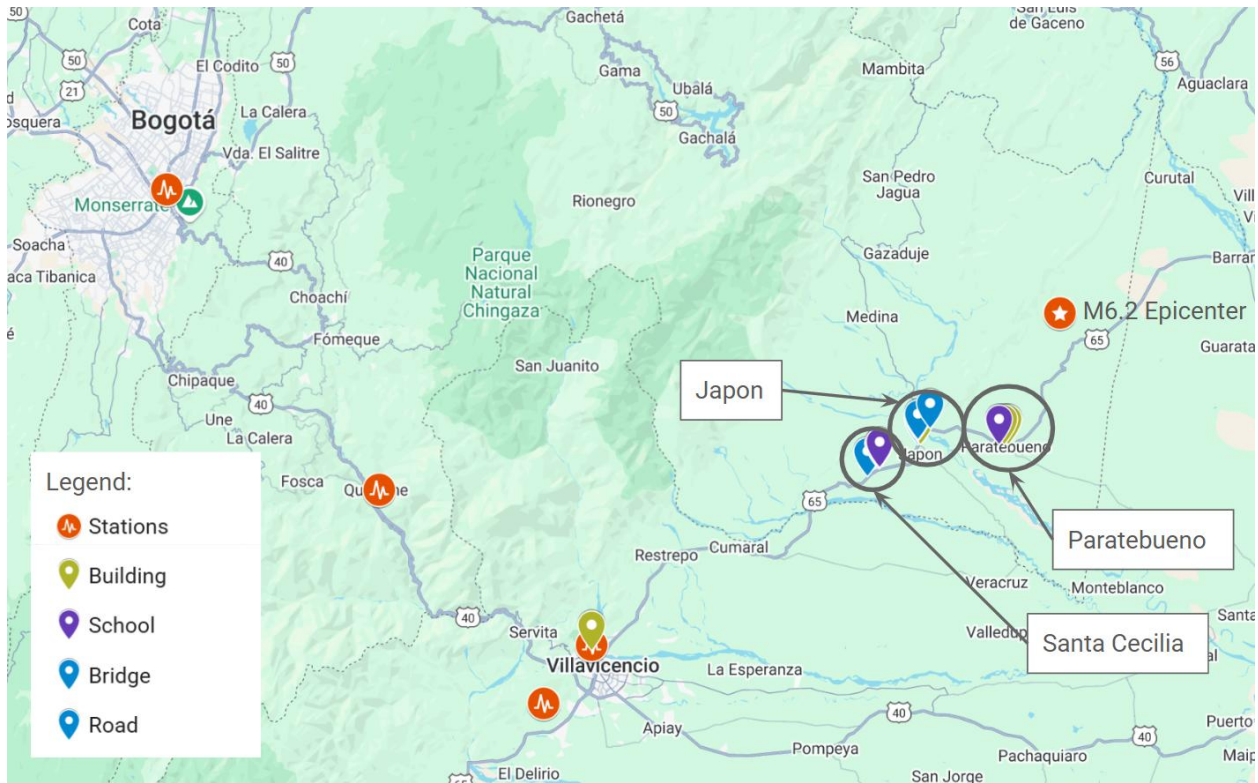


Figure 4.1. Locations visited by CEER FAST on June 12, 2025.

4.2. Single-family Residential Houses

Most of the damage was concentrated in non-engineered single-family housing, typically a single story in height. Single-family homes experienced various levels of damage ranging from severe wall cracking to complete collapse. Unsurprisingly, many of the collapses occurred in houses made of unreinforced masonry. Figure 4.2 highlights examples of these common failure modes.

No total collapses were observed in single-story houses that utilized a partially-confined masonry system. Figure 4.3 shows the behavior of two single-story houses built on the same block: one damaged partially-confined masonry house and one collapsed URM house.

While surveying a residential area in Japon, a local resident invited the team to inspect a house that had suffered visible damage during the earthquake. One of the rooms, fortunately unoccupied at the time of the event, experienced a complete collapse of one of its masonry walls. The debris covered much of the interior space, and had anyone been inside, the consequences could have been severe or even fatal (see Figure 4.4).

Adjacent to the main house, the team observed a makeshift outdoor kitchen structure supported by slender masonry piers constructed with hollow clay blocks and mortar, without any apparent reinforcement. These vertical elements suffered significant cracking and crushing; the structure appeared extremely vulnerable to aftershocks or even minor disturbances (see Figure 4.5).



Figure 4.2. Examples of URM single family house collapse in Santa Cecilia (Credit: Archbold and Carrillo).



Figure 4.3. Comparing damage of a partially-confined masonry house (left) compared to an unreinforced masonry house on the same block in Santa Cecilia (Credit: Archbold and Carrillo).



Figure 4.4. Interior view of a collapsed masonry wall in residence in Japón, Cundinamarca; room was unoccupied at the time of the earthquake, preventing potential injury (Credit: Archbold and Carrillo).



Figure 4.5. Severely damaged outdoor kitchen structure outside residence in Japón, Cundinamarca; structure was supported by unreinforced masonry piers (Credit: Archbold and Carrillo).

Typical reinforced concrete (RC) frames were observed in both residential and commercial areas. This structural system consists of RC beams and columns to resist both lateral and vertical loads. The floor systems are typically solid or hollow-brick masonry slabs, and the infill walls are commonly made of concrete or clay masonry units. This system generally performed well with no visible damage or collapses were observed (see example in Figure 4.6).



Figure 4.6. Performance of a two-story concrete frame house with infill walls in Japon, Cundinamarca (Credit: Carrillo).

4.3. Commercial Buildings

Soft- or weak-story failure was observed in the ground-floor collapse of a two-story mixed concrete and steel frame commercial building with infill walls (see Figure 4.7 for before-and-after images of the structure). This type of failure can occur due to inadequate connections between concrete and/or steel elements, as illustrated in Figure 4.8.



(a)



(b)

Figure 4.7. Family-owned business Siete Cueros in Santa Cecilia, Paratebueno: (a) before the seismic event (Source: Google Maps) and (b) after the event (Source: El Espectador, 2025).

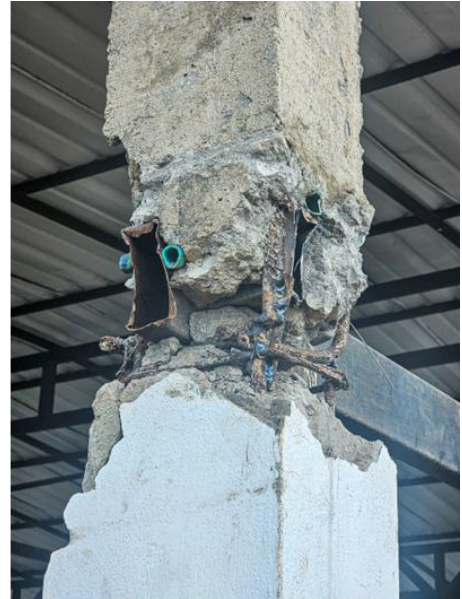


Figure 4.8. Structural details observed in collapse of the Siete Cueros commercial building in Santa Cecilia, Paratebueno—same site shown in Figure 4.7 (Credit: Archbold and Carrillo).

4.4. Performance of School Buildings

Preliminary reports mention damage in at least 24 schools in the affected area of the department of Cundinamarca, including several instances of complete structural collapse. Fortunately, no

child casualties have been reported, as the earthquake occurred on a Sunday. One critical case was Santa Cecilia School, located approximately 15 km west of Paratebueno, where at least four of the buildings collapsed. Figure 4.9 shows several of the school's structures, with a post-earthquake aerial view on the left and pre-earthquake building details on the right. The building in the yellow box is a reinforced frame structure that did not show any visible damage despite the large openings and short columns. The structures inside the red and green boxes are both masonry structures with similar characteristics; however, the one outlined with the red rectangle completely collapsed while the other remained standing. Notably, an addition on the right side of the collapsed structure, which appeared to be a well-confined masonry structure, also collapsed.

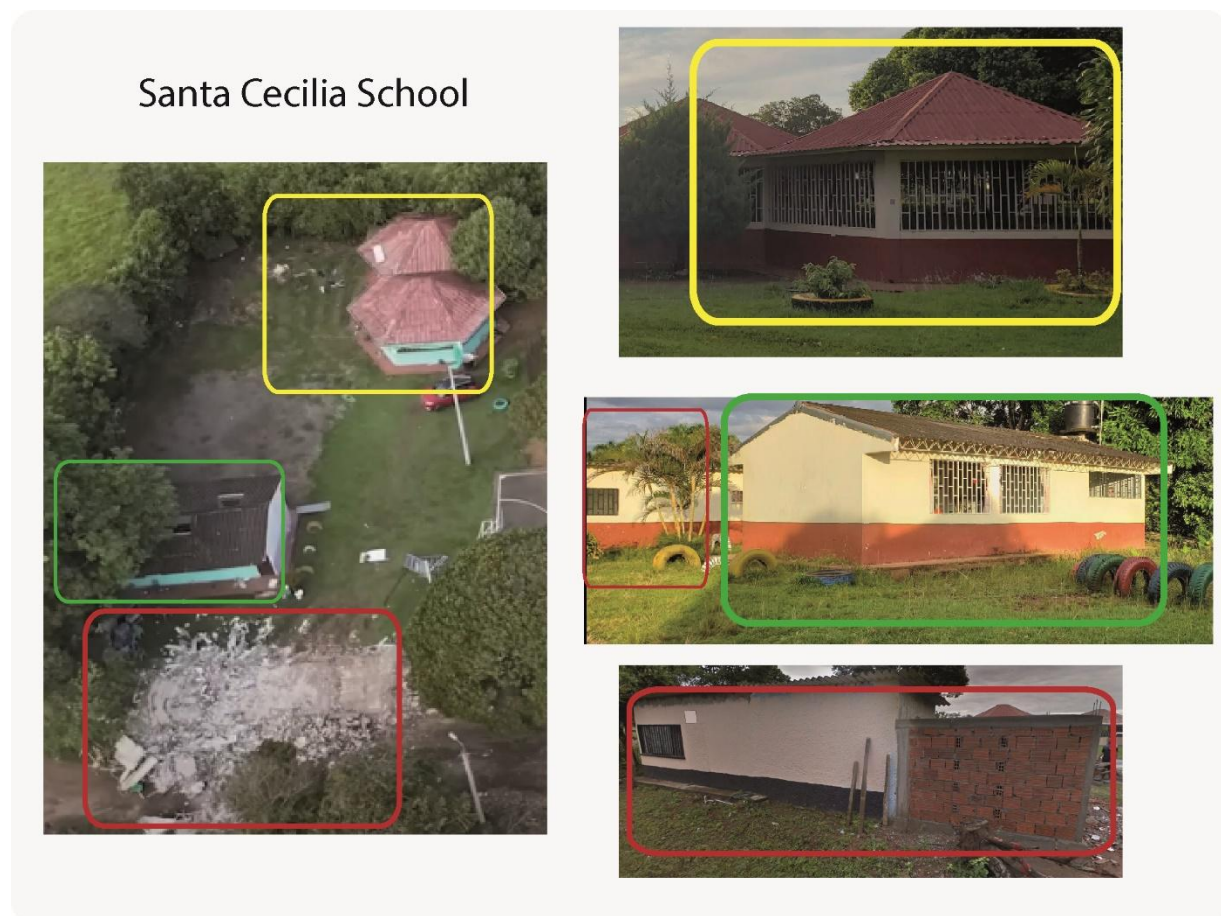


Figure 4.9. General view of Santa Cecilia School. Building of the school (left) after the earthquake (Source: El tiempo, 2025b) and (right) details of the structures (Source: Google Maps).

Other buildings that also collapsed within the same school complex are shown in Figure 4.10. The top and bottom images depict the buildings prior to the earthquake. These structures were constructed with horizontally perforated clay bricks and cement mortar, as confirmed by the

examination of the collapsed rubble on site. The middle image shows interior details of one of the collapsed buildings. The yellow rectangle highlights the collapsed façade, which overturned as a rigid body. The green rectangle indicates a wall perpendicular to the façade, revealing a lack of sufficient elements to restrain the out-of-plane deformation of the façade. The roof did not collapse, as the concrete frame—highlighted in the red rectangle—remained intact and continued to support the roof structure.



Figure 4.10. Collapsed buildings in Santa Cecilia School and details of the collapse: (top) structure before the earthquake (Source: IEDR Santa Cecilia, 2025); (middle) damages and collapse of the school (Source: Facebook, 2025); (bottom) school module before the earthquake (Source: Google Maps).

Figure 4.11 shows examples of damage and disruption observed by the CEER FAST. In Figure 4.11a and b, a one-story reinforced concrete moment-frame classroom building is shown with no visible structural damage. An adjacent classroom, shown in Figure 4.11c, sustained non-structural damage, including partial ceiling collapse. On the blackboard, the date of the last class held before the earthquake—June 6, 2025—is still visible. In Figure 4.12d, broken laptops from government programs aimed at providing computers to rural schools can be seen scattered on the floor.



(a)



(b)



(c)



(d)

Figure 4.11. (a–b) One-story reinforced concrete moment-frame classroom building with no visible structural damage; (c) Non-structural damage observed inside a classroom; (d) Broken laptops found on the floor; one bears the inscription “Computers to Educate” (Credit: Archbold and Carrillo).

Damaged schools in the region share similar characteristics, as exemplified by a school located in the community of Japón, approximately 10 km west of Paratebueno. In Figure 4.12, the top image shows the school before the earthquake. All the buildings are made of masonry; however, those highlighted by the yellow rectangle were built more than 40 years ago using concrete bricks. In contrast, the structure outlined by the green rectangle, which did not suffer significant damage, was built in the 1990s and incorporates reinforced concrete elements to confine the masonry. A more modern single-story building in the same school, constructed entirely of reinforced concrete, also remained undamaged.



Figure 4.12. Collapsed and undamaged buildings at Japón municipality school campus: (top) structure before earthquake (Source: Google Maps); (bottom) collapsed building (Credit: Archbold and Carrillo).

4.5. Religious Institutions

The Catholic church in the town center of Santa Cecilia, Paratebueno, was one of the most visibly affected religious structures observed by the FAST. The team documented severe structural and non-structural damage, including major cracking in load-bearing masonry walls and columns, localized collapse of plaster finishes, and visible signs of roof misalignment. The extent of the damage rendered the building unsafe for use, and parts of the interior were inaccessible at the time of inspection (see Figure 4.13). As a central gathering space for the community, the church's closure has had a notable social and emotional impact on residents.



(a)



(b)



(c)



(d)

Figure 4.13. Damage to the church at Santa Cecilia: (a) front façade, (b) side view, (c) rear view, and (d) interior of church (Credit Archbold and Carrillo).

Although the team did not visit Pandi, Cundinamarca, independent reports confirmed that its main church also sustained earthquake-related damage. A photograph shared by the Cundinamarca Risk Management Office (RiesgosCundi, 2025) shows visible cracking in internal wall (see Figure 4.14).

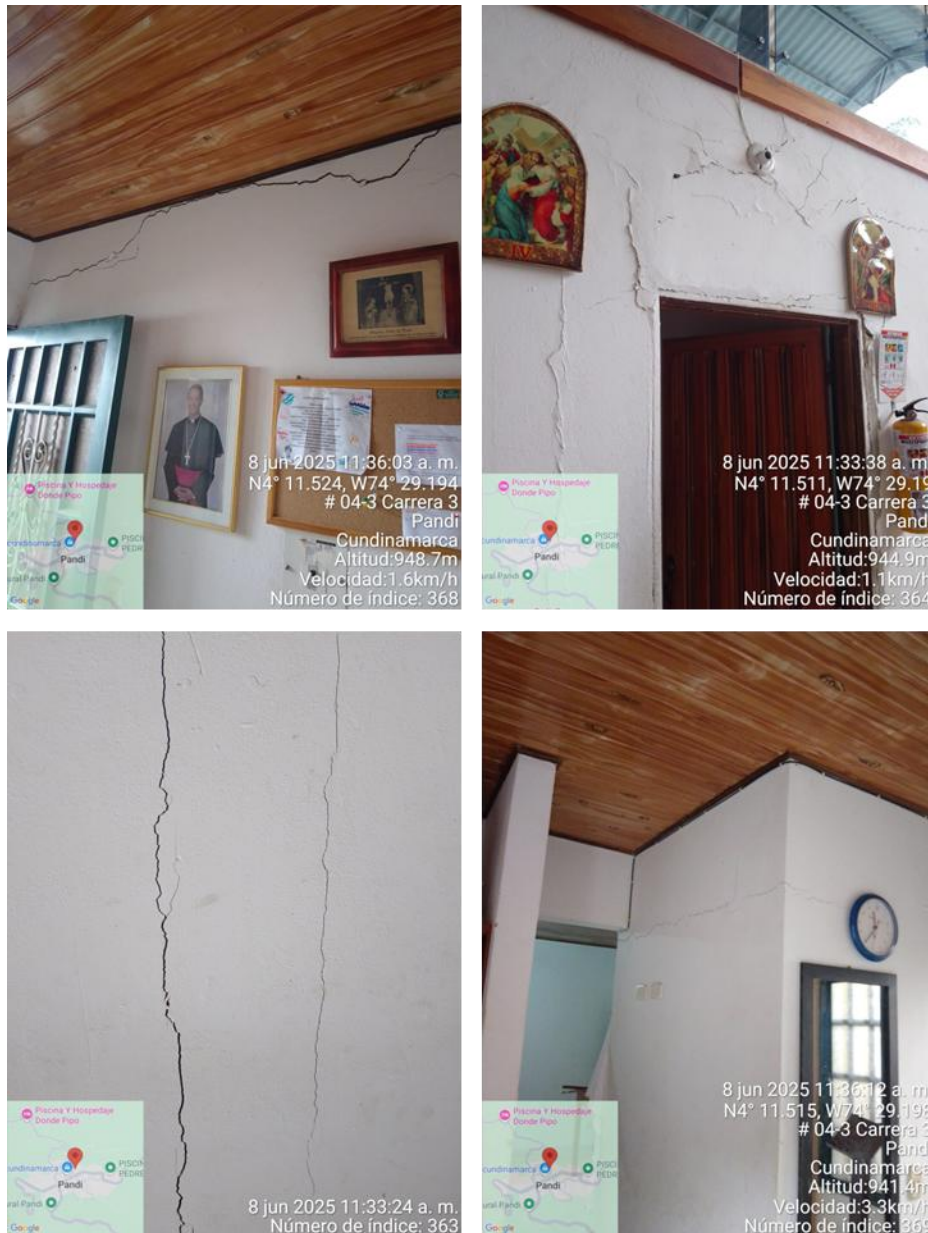


Figure 4.14. Observed damaged at the town’s church in Pandi, Cundinamarca (Source: RiesgosCundi, 2025).

4.6. Site Walls

Out-of-plane collapse of masonry site walls was observed in Paratebueno (Figure 4.15). The main causes of this failure were: (i) a lack of sufficiently reinforced beams and columns to resist overturning moment due to out-of-plane loads and provide confinement for the unreinforced masonry panels, and (ii) the use of bricks with insufficient strength.



Figure 4.15. Failure of site walls in Paratebueno (Credit Archbold and Carrillo).

5. Infrastructure Performance

The June 8, 2025, Paratebueno earthquake affected some local infrastructure systems between the towns of Japón and Paratebueno, disrupting mobility and highlighting both their vulnerability and resilience of engineered systems. This section focuses on the performance of bridges, which were among the most visibly and structurally consequential components impacted by the event. The FAST documented damage to three reinforced concrete bridges along the Cumaral–Paratebueno corridor, a critical transportation route in the region (refer back to Figure 4.1 for map of the structures surveyed relative to the SGC ground motion stations). These included a multi-span vehicular bridge, a single-span bridge, and a pedestrian overpass. Observations revealed varying levels of damage associated with shear key failure, abutment settlement, pounding between spans and approaches, and evidence of possible ground failure such as liquefaction and lateral spreading.

Detailed photographic and field evidence is presented in the following subsections, organized by bridge type. The case studies include:

1. Puente Río Humea, a three-span vehicular bridge that experienced shear key failures and bearing displacements, leading to a temporary road closure;
2. A single-span beam bridge in the town of Japón, where abutment settlement and cracking were observed; and
3. A reinforced concrete pedestrian bridge, which suffered damage to shear keys and exhibited signs of pounding and deck displacement.

5.1. Three-span Vehicular Traffic Bridge

The Puente Río Humea, a three-span reinforced concrete bridge along the Cumaral–Paratebuena road, remained closed for five days after the earthquake and was reopened with controlled traffic after June 13, 2025 (Casanare Noticias, 2025). The bridge deck impacted the shear keys, a mechanism that effectively prevented the unseating of the superstructure. One of the abutment’s shear keys experienced significant damage, presenting a diagonal shear failure in its stem wall, as shown in Figure 5.1. This type of failure is commonly observed in monolithic shear keys.

The horizontal gap at the top of this severely damaged shear key was measured between 16 cm and 21 cm, accompanied by a crack of an approximately 9 cm width and evidence of rebar buckling. These values suggest that the lateral displacement of the bridge deck impacting the shear key was roughly 7 cm. In contrast, other shear keys on the bridge exhibited horizontal shear fractures (Figure 5.2), a failure mechanism considered more desirable for post-earthquake repair. Its occurrence suggests that the amount of vertical reinforcement connecting the shear key to the stem wall was relatively small, and that the stem wall possessed adequate horizontal shear reinforcement, enabling this more favorable failure response.

The bridge appears to use two types of bearings: circular rubber bearings on top of the two midspan piers (Figure 5.3) and square expansion bearings at the abutments (Figure 5.5). The bearings on the piers show no visible damage and may have protected the piers from excessive seismic demands, as no significant structural damage was visible (Figure 5.4). However, the steel jacket at one of the piers exhibited damage (Figure 5.4), though the pre-earthquake condition of this jacket remains unknown.

Figure 5.6 shows evidence of the uplift of some abutment bearings from their seats. Figure 5.5 also highlights residual displacement in the abutment bearings, indicating both longitudinal and transverse displacement of the bridge deck relative to the abutment. The gap between the bearing and its seat may be due to the span climbing longitudinally onto the abutment during the earthquake. Alternatively, the gap could be attributed to abutment rotation induced by soil failure. Figure 5.7 presents evidence of such rotation, along with signs of differential settlement and lateral spreading around the abutments.



Figure 5.1. Puente Río Humea: shear key with a diagonal shear failure in the stem wall (Credit: Archbold and Carrillo).



Figure 5.2. Puente Río Humea: shear keys with a horizontal shear failure mechanism (Credit: Archbold and Carrillo).



ceer
COLOMBIAN EARTHQUAKE ENGINEERING RESEARCH NETWORK

UNIVERSIDAD
EIA
Ser. Sabery Servir



UNIVERSIDAD DE MEDELLIN
Resolución Institucional
Resolución N° 10006 del 12 de agosto de 2013 - Vigencia 6 años



UNIVERSIDAD MILITAR
NUEVA GRANADA
"La U para todos"



Universidad
del Valle



Universidad
Industrial de
Santander



UNIVERSIDAD
DEL NORTE
Vigilada por el Ministerio de Educación



Figure 5.3. Puente Río Humea: midspan bridge bearings (Credit: Archbold and Carrillo).



Figure 5.4. Puente Río Humea: bridge piers with steel jackets (Credit: Archbold and Carrillo).





Figure 5.5. Puente Río Humea: abutment bearings longitudinal and transverse movement (Credit: Archbold and Carrillo).



Figure 5.6. Puente Río Humea: abutment bearings vertical uplifting (Credit: Archbold and Carrillo).



Figure 5.7. Puente Río Humea: damage around the abutments and signs of lateral spreading (Credit: Archbold and Carrillo).

5.2. Single-span Vehicular Traffic Bridge

One of the bridges assessed was a single-span, reinforced concrete beam bridge designed for vehicular traffic, located in the town of Japón along the Cumaral–Paratebuena road. Figure 5.8 shows an unusual abutment seat detail, where a piece of wood—possibly formwork left in place during construction—remains embedded in the concrete. This detail is included to document the

deck-to-abutment interface, which may be relevant for further structural evaluation. Damage observed at the site included a large vertical crack on one of the abutments likely caused by differential settlement (Figure 5.9, left and center). Signs of ground settlement can be noted on the right side of the abutment (Figure 5.9, center), suggesting differential foundation movement. A thinner vertical crack was also observed on the other abutment (Figure 5.9, right); however, it is unclear if this crack was related to recent settlement or if it predated the earthquake event. Minor spalling was present on sections of the concrete barriers.



Figure 5.8. Abutment seat detail of bridge along the Cumaral–Paratebueno road in Japón (Credit: Archbold and Carrillo).



Figure 5.9. Vertical crack of the abutment due to differential settlement of bridge along the Cumaral–Paratebueno road in Japón (Credit: Archbold and Carrillo).

5.3. Pedestrian Bridge

A reinforced concrete pedestrian bridge on the main highway connecting Cumaral with Paratebueno, near the entrance to the town of Japón, Cundinamarca, approximately 22 km from the epicenter, was closed to the public following the earthquake (Figure 5.10). Damage to the bridge included failure of the shear keys: two exhibited a diagonal shear fracture, while the other two displayed a horizontal shear failure (Figure 5.11). Some non-structural damage was observed on the drainage pipe adjacent to the bridge. Evidence of pounding between the deck and the ramp of the pedestrian bridge was also noted, along with a possible fracture of the cantilevered approach structure (Figure 5.12). In addition, debris was found below the pier cap due to the spalling of the shear keys (Figure 5.13).



Figure 5.10. Pedestrian Bridge along main highway connecting Cumaral with Paratebueno, near the entrance to town of Japón, Cundinamarca (Credit: Archbold and Carrillo).

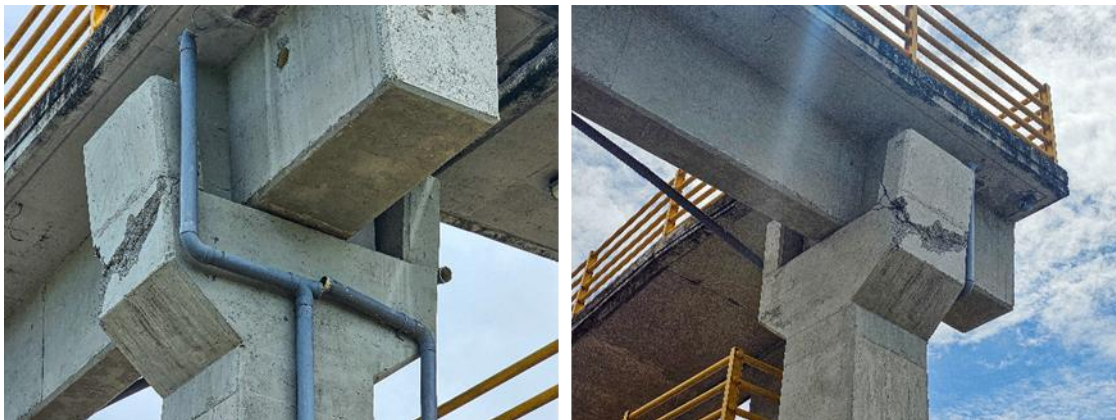


Figure 5.11. Pedestrian bridge along main highway connecting Cumaral with Paratebueno, near the entrance to town of Japón, Cundinamarca: shear keys with diagonal shear failure (Credit: Archbold and Carrillo).



Figure 5.12. Pedestrian bridge along main highway connecting Cumaral with Paratebueno, near the entrance to town of Japón, Cundinamarca: signs of pounding between the ramp and the deck of the bridge (Credit: Archbold and Carrillo).



Figure 5.13. Pedestrian bridge along main highway connecting Cumaral with Paratebueno, near the entrance to town of Japón, Cundinamarca: fallen debris from the pier cap spalling (Credit: Archbold and Carrillo).

6. Geotechnical Performance

The earthquake triggered significant geotechnical damage in the region. Notably, the seismic event reactivated a large translational landslide affecting more than 60 hectares (0.60 km²) of terrain near the Cumaral–Paratebueno corridor, as shown in Figure 6.1 (SGC, 2025a, 2025d). The landslide measured approximately 380 meters wide at the crown and extended 1.5 kilometers in length from crown to toe, with a main scarp height of about 60 meters. Field assessments indicate that the landslide mass consisted primarily of clayey soils, which exhibit high sensitivity to variations in moisture content (El Tiempo, 2025a). In comparison, the area exposed to landslide hazard was slightly overestimated by the USGS PAGER system, which estimated landslide-affected terrain of 1 to 10 km² (USGS, 2025a).



Figure 6.1. Earthquake-induced landslide near the municipality of Paratebueno (Sources: SGC, 2025a, 2025d).

As a result of the landslide, the Caño Grande stream was entirely occluded, resulting in the complete loss of its natural channel morphology. The landslide also partially blocked the Naguaya stream, causing upstream impoundment and raising concerns about potential outburst flooding. In addition to its hydrological impacts, the landslide caused significant infrastructure damage (Covioriente, 2025a), including the disruption of the rural access road to Medina and the displacement of utility poles located near the landslide crown. The event also resulted in several ground surface tension cracks and widespread treefall over approximately 0.70 km², with some trees reportedly collapsing onto neighboring rural residences (see Figure 6.2). According to TV news reports, the entire La Europa hamlet near Paratebueno may have been wiped out by the landslide (Noticias Caracol, 2025).



Figure 6.2. Damage associated with the landslide: (a) tree collapsed onto a rural structure; (b) tension cracks and surface fissures observed near the landslide (Source: Instagram @serviciogeologicocolombiano, 2025).

USGS also estimated a high probability (> 20%) of liquefaction occurring in the low-lying plains southeast of the range front, near the municipalities of Medina, Paratebueno, and the rural areas in the Department of Meta (see Figure 6.3). However, no official confirmations or field reports of liquefaction have been released by SGC or other governmental agencies as of this report's release.

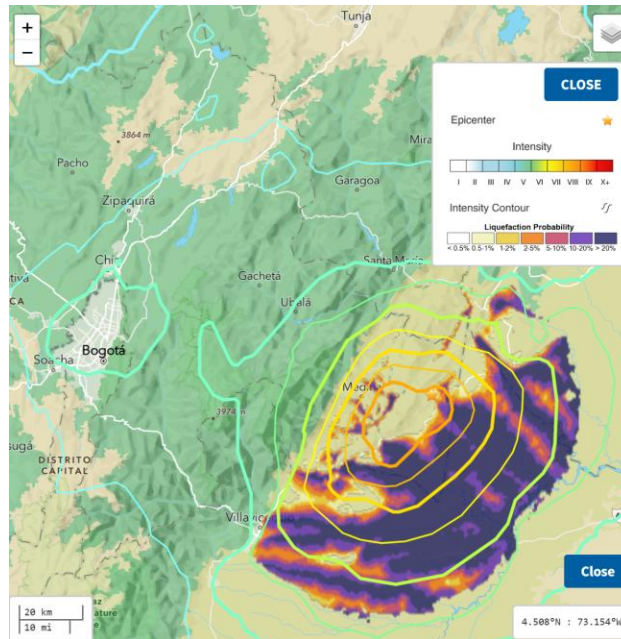


Figure 6.3. Estimated probability of liquefaction (Source: USGS, 2025a).

7. Recommended Response Strategy

Based on the information gathered in this report, the authors offer the following recommendations for future study.

TOPIC 1: Risk Assessment of Informal and Non-Engineered Buildings

A significant portion of the structural damage observed during the Paratebueno earthquake occurred in informal or non-engineered buildings. These structures were predominantly self-built, lacked adherence to seismic design regulations, and were not supervised by qualified professionals. This building typology is prevalent not only in rural areas but also on the outskirts of major urban centers across South America. Future research should focus on the development and deployment of rapid visual screening methodologies supported by low-cost, user-friendly technological tools, such as mobile applications, drone-based inspections, or AI-assisted image processing. These tools would enable broad-scale, preliminary structural assessments to identify high-risk buildings and inform subsequent, more detailed evaluations. Ultimately, the goal is to establish data-driven prioritization mechanisms to support timely decision-making by local and national authorities.

TOPIC 2: National Risk Assessment Model for Educational Infrastructure

The extensive damage to educational facilities during the earthquake highlights the urgent need for a systematic evaluation of the school buildings across the country. The vulnerability identified by the CEER technical team, linked to both structural characteristics and adverse geotechnical

conditions, demonstrates the high seismic risk faced by students and educational communities. Future studies should contribute to the formulation of a National Risk Assessment Model for Educational Infrastructure in Colombia, which must integrate structural, geotechnical, and social vulnerability indicators. This model should be used to develop evidence-based risk reduction and mitigation strategies, including retrofitting guidelines, safe site selection, and resource allocation. Such a framework must be adaptable to regional conditions and continually informed by the lessons learned from events like the Paratebueno earthquake.

TOPIC 3: Resilience of Lifelines and Rural Communities

The Paratebueno earthquake caused significant disruptions to critical lifelines, including severe damage to road infrastructure and bridges, power outages in the epicentral area, and interruptions in telecommunications services. These impacts underscore the heightened vulnerability of rural communities, where remoteness and limited access to basic services exacerbate the consequences of seismic events. Future studies should prioritize the development of strategies aimed at strengthening the resilience of rural communities through improved emergency preparedness, local response capacity, and coordinated efforts between community members and regional authorities. In parallel, it is imperative to advance a national strategy for the maintenance and conservation of bridge infrastructure, recognizing that many bridges across Colombia exhibit significant deterioration even under normal service conditions. Integrating periodic inspections and vulnerability assessments with structural health monitoring technologies and non-destructive evaluation should be central to these efforts to ensure that critical transport infrastructure remains functional before, during, and after seismic events.

ESCALATION DECISION

Based on the nature of the damage and the characteristics of the event, the authors do not recommend that StEER escalate its response and deploy additional **Field Assessment Structural Teams**. Although the damage was extensive, it was largely concentrated in non-engineered structures such as unreinforced masonry and informal housing, which, unfortunately, is consistent with expectations for the building stock in the affected region. There was no evidence of widespread collapse in engineered structures or significant damage to high-occupancy or critical facilities that would warrant an escalation.

Consequently, this JRR represents the extent of StEER’s official response; however, StEER will continue to support its Colombian colleagues, particularly those in CEER, in their continued study of this event to encourage consideration of the above recommendations and will monitor their assessments. Should these ongoing efforts reveal new information that would satisfy one or more of StEER’s escalation criteria, StEER may re-evaluate its decision and deploy a FAST.

References

- AIS. (1984). Código Colombiano de Construcciones Sismo Resistentes (Decreto 1400 de Junio 7 de 1984). In. Bogotá, Colombia: Asociación Colombiana de Ingeniería Sísmica.
- AIS. (1996). Estudio General de Amenaza Sísmica de Colombia. In. Bogotá, Colombia: Asociación Colombiana de Ingeniería Sísmica.
- AIS. (1998). Normas Colombianas de Diseño y Construcción Sismo Resistentes, NSR-98. In. Bogotá, Colombia: Asociación Colombiana de Ingeniería Sísmica.
- AIS. (2009). Estudio General de Amenaza Sísmica de Colombia 2009. In. Bogotá, Colombia: Asociación Colombiana de Ingeniería Sísmica.
- Arteta, C. A., & Caballero, J. (2025). (2025, June 10). *Fast report of observed ground-motion trends: M6.4 – 12 km NNE of Paratebueno, Colombia [Technical report]*. Retrieved from Colombian Earthquake Engineering Research Network (CEER), Universidad del Norte. : <https://www.ceer.co>
- Arteta, C. A., Pajaro, C. A., Mercado, V., Montejo, J., Arcila, M., & Abrahamson, N. A. (2021). Ground-motion model for subduction earthquakes in northern South America. *Earthquake Spectra*, 37(4), 2419-2452. doi:10.1177/87552930211027585
- Arteta, C. A., Pajaro, C. A., Mercado, V., Montejo, J., Arcila, M., & Abrahamson, N. A. (2023). Ground-Motion Model (GMM) for Crustal Earthquakes in Northern South America (NoSAM Crustal GMM). *Bulletin of the Seismological Society of America*, 113(1), 186-203. doi:10.1785/0120220168
- Blu Radio. (2025a). Familias de Paratebueno y Medina recibirán subsidios y nuevos hogares tras el sismo. Retrieved from <https://www.bluradio.com/regiones/cundinamarca/familias-de-paratebueno-y-medina-recibiran-subsidios-y-nuevos-hogares-tras-el-sismo-so35>
- Blu Radio. (2025b). La tierra se mueve en Paratebueno: reubicarán a 80 familias por gigantesco deslizamiento por temblor. Retrieved from <https://www.bluradio.com/regiones/cundinamarca/la-tierra-se-mueve-en-paratebueno-reubicaran-a-80-familias-por-gigantesco-deslizamiento-por-temblor-rg10>
- Campbell, K. W. (1997). Empirical Near-Source Attenuation Relationships for Horizontal and Vertical Components of Peak Ground Acceleration, Peak Ground Velocity, and Pseudo-Absolute Acceleration Response Spectra. *Seismological Research Letters*, 68(1), 154-179. doi:10.1785/gssrl.68.1.154
- Caracol Radio. (2025). "La reconstrucción de Paratebueno ya comenzó, pero necesitamos más ayuda": Gobernador Rey. Retrieved from <https://caracol.com.co/2025/06/17/la-reconstruccion-de-paratebueno-ya-comenzo-pero-necesitamos-mas-ayuda-gobernador-rey/>
- Carrillo, J., Blandón-Valencia, J., & Rubiano, A. (2013). A review of conceptual transparency in US and Colombian seismic design building codes. *Ingeniería e Investigación*, 33, 24-29. Retrieved from http://www.scielo.org.co/scielo.php?script=sci_arttext&pid=S0120-56092013000200005&nrm=iso
- Casanare Noticias. (2025). Fue habilitado paso controlado por el puente sobre el Río Humea. Retrieved from <https://www.casanarenoticias.com/index.php/regional/item/22393-fue-habilitado-paso-controlado-por-el-puente-sobre-el-rio-humea>
- Colombia.com. (2025). Damnificados del temblor en Paratebueno quedaron desamparados: carpa quedó destruida tras vendaval. Retrieved from

- <https://www.colombia.com/actualidad/nacionales/damnificados-del-temblor-en-paratebueno-pierden-su-unico-refugio-por-venda-525112>
- Covioriente. (2025a). Activación del Plan de Gestión Preventiva de Riesgo en el sector La Europa Retrieved from <https://www.covioriente.co/activacion-del-plan-de-gestion-preventiva-de-riesgo-en-el-sector-la-europa/>
- Covioriente. (2025b). Covioriente evalúa y atiende situación presentada por sismo en Paratebueno sobre la vía nacional. Retrieved from <https://www.covioriente.co/covioriente-evalua-y-atiende-situacion-presentada-por-sismo-en-paratebueno-sobre-la-via-nacional/>
- Earthquake Spectra. (2025). National Seismic Risk Model of Colombia Special Collection. Retrieved from <https://journals.sagepub.com/topic/collections-egs/egs-1-national-seismic-risk-model-of-colombia/egs>
- El Espectador. (2025). Cuatro heridos y varios daños dejó temblor en Paratebueno y otros municipios. Retrieved from <https://www.elespectador.com/colombia/cundinamarca/cuatro-heridos-y-varios-danos-dejo-temblor-en-paratebueno-y-otros-varios/>
- El Tiempo. (2025a). La vereda que casi desaparece por deslizamiento tras temblor en Paratebueno: familias serán reubicadas. Retrieved from <https://www.eltiempo.com/bogota/la-vereda-que-casi-desaparece-por-deslizamiento-tras-temblor-en-paratebueno-familias-seran-reubicadas-3463857>
- El tiempo. (2025b). 'Nuestros sueños, esfuerzo y trabajo quedaron hechos escombros': víctimas del temblor en Paratebueno. Retrieved from <https://www.eltiempo.com/bogota/nuestros-suenos-esfuerzo-y-trabajo-quedaron-hechos-escombros-victimas-del-temblor-en-paratebueno-3463414>
- El Tiempo. (2025c). Temblor en Colombia | Meta y Cundinamarca tienen graves afectaciones: daños en el 90% de viviendas de Santa Cecilia. Retrieved from <https://www.eltiempo.com/colombia/otras-ciudades/temblor-en-colombia-meta-y-cundinamarca-sufrieron-graves-afectaciones-el-90-de-las-viviendas-de-santa-cecilia-sufrieron-danos-3461698>
- Facebook. (2025). @La Original Mix #cundinamarca La escuela rural de la vereda Santa Cecilia, en el municipio de Paratebueno (Cundinamarca), quedó completamente destruida tras el fuerte sismo de magnitud 6.5 registrado este 8 de junio. Retrieved from <https://web.facebook.com/watch/?v=1110186927603793>
- Grünthal, G. (1998). *European Macroseismic Scale 1998 (EMS-98)*. Retrieved from IEDR Santa Cecilia. (2025). INSTITUCION EDUCATIVA DEPARTAMENTAL RURAL SANTA CECILIA. Retrieved from <https://iedrsantacecilia.wordpress.com/>
- infobae. (2025). Sismo en Bogotá: falso que puente en exclusivo sector resultó averiado. Retrieved from <https://www.infobae.com/colombia/2025/06/09/sismo-en-bogota-falso-que-puente-en-exclusivo-sector-resulta-averiado/>
- Instagram (@serviciogeologicocolombiano) [serviciogeologicocolombiano]. (2025). [Instagram]. Retrieved from <https://www.instagram.com/p/DLEAPf3saqj/>
- Mercado, V., Díaz-Parra, F. J., Pajaro, C. A., Montejo, J., Posada, G., Arcila, M., & Arteta, C. A. (2024). Performance evaluation of parameters as estimators of seismic site effects in northern South America. *Soil Dynamics and Earthquake Engineering*, 180, 108584. doi:<https://doi.org/10.1016/j.soildyn.2024.108584>

- Mercado, V., Pajaro, C. A., Arteta, C. A., Díaz, F. J., Montejo, J., Arcila, M., & Abrahamson, N. A. (2023). Semiempirical model for the estimation of site amplification in Northern South America. *Earthquake Spectra*, 39(2), 1109-1139. doi:10.1177/87552930231153190
- Ministerio de Ambiente, Vivienda y Desarrollo Territorial. (2010). Reglamento Colombiano de Construcción Sismo Resistente NSR-10. In. Bogotá, Colombia: Asociación Colombiana de Ingeniería Sísmica.
- Noticias Caracol (2025). Tras temblor en Paratebueno, Cundinamarca, ahora hay riesgo de deslizamiento [Youtube]. Retrieved from https://www.youtube.com/watch?v=V4_aac9djYw
- Pajaro, C. A. (2024). *Development of ground motion models for Northern South América - NoSAM GMMs*. (Doctoral dissertation). Universidad del Norte.
- Pajaro, C. A., Arteta, C. A., Mercado, V., Montejo, J., Arcila, M., & Abrahamson, N. A. (2024). Partially non-ergodic ground motion model for the Bucaramanga seismic nest in Northern South America (NoSAM Nest GMM). *Bulletin of Earthquake Engineering*, 22(8), 3677-3702. doi:10.1007/s10518-024-01898-w
- Presidencia de la Republica de Colombia. (2025a). Sismo del domingo 8: asistencia humanitaria y carrotanque de UNGRD ya están en Paratebueno. Retrieved from <https://www.presidencia.gov.co/prensa/Paginas/Sismo-del-domingo-8-asistencia-humanitaria-y-carrotanque-de-UNGRD-ya-estan-250612.aspx>
- Presidencia de la Republica de Colombia. (2025b). Unidad de Gestión del Riesgo y Bomberos reportan balance de daños tras fuerte sismo en Paratebueno. Retrieved from <https://www.presidencia.gov.co/prensa/Paginas/Unidad-de-Gestion-del-Riesgo-y-Bomberos-reportan-balance-de-danos-tras-fuer-250608.aspx>
- RiesgosCundi (2025). #Pandi Agrietamiento iglesia en cabecera municipal [X]. Retrieved June 27, 2025
- Sarabia Gómez, A. M., Barbosa Castro, D. R., & Arcila Rivera, M. M. (2022). Macroseismic intensity data and effects of significant earthquakes in Colombia based on historical seismicity studies. *Boletín Geológico*, 49(2), 5-14. doi:10.32685/0120-1425/bol.geol.48.2.2021.638
- SGC. (2025a). Deslizamientos en la vereda La Europa (Paratebueno), tras el sismo del 8 de junio. Retrieved from <https://www2.sgc.gov.co/Noticias/Paginas/Deslizamientos-en-la-vereda-La-Europa-Paratebueno-tras-el-sismo-del-8-de-junio.aspx>
- SGC. (2025b). Paratebueno – Cundinamarca, Colombia. Intensidad Percibida. Retrieved from <https://www.sgc.gov.co/detallesismo/SGC2025lfawhz/cdi>
- SGC. (2025c). Paratebueno – Cundinamarca, Colombia. Servicio Geologico Colombiano Retrieved from <https://www.sgc.gov.co/detallesismo/SGC2025lfawhz/resumen>
- SGC. (2025d). Sismo de Paratebueno reactivó movimiento en masa de 60 hectáreas, cerca a la vía Cumaral. Retrieved from <https://www2.sgc.gov.co/Noticias/Paginas/Sismo-de-Paratebueno-reactivo-movimiento-en-masa-de-60-hectareas-cerca-a-la-via-Cumaral.aspx>
- Survey, G., & Paris, G. (2000). *Map and database of Quaternary faults and folds in Colombia and its offshore regions*: US Geological Survey.
- Taboada, A., Rivera, L. A., Fuenzalida, A., Cisternas, A., Philip, H., Bijwaard, H., . . . Rivera, C. (2000). Geodynamics of the northern Andes: Subductions and intracontinental deformation (Colombia). *Tectonics*, 19(5), 787-813. doi:<https://doi.org/10.1029/2000TC900004>



UNGRD. (2025). UNGRD envía asistencia humanitaria y equipos técnicos a Paratebueno y Medina tras emergencia. Retrieved from <https://portal.gestiondelriesgo.gov.co/Paginas/Noticias/2025/UNGRD-envia-asistencia-humanitaria-y-equipos-tecnicos-a-Paratebueno-y-Medina-tras-emergencia.aspx>

USGS. (2025a). M 6.3 - 15 km NE of Paratebueno, Colombia (Ground Failure). Retrieved from <https://earthquake.usgs.gov/earthquakes/eventpage/us6000qixr/ground-failure/summary>

USGS. (2025b). M 6.3 - 15 km NE of Paratebueno, Colombia (Overview). Retrieved from <https://earthquake.usgs.gov/earthquakes/eventpage/us6000qixr/executive>

USGS. (2025c). M 6.3 - 15 km NE of Paratebueno, Colombia (PAGER). Retrieved from <https://earthquake.usgs.gov/earthquakes/eventpage/us6000qixr/pager>

Worden, C. B., Gerstenberger, M. C., Rhoades, D. A., & Wald, D. J. (2012). Probabilistic Relationships between Ground-Motion Parameters and Modified Mercalli Intensity in California. *Bulletin of the Seismological Society of America*, 102(1), 204-221. doi:10.1785/0120110156